ABSTRACT

HENDRIX, ANGELEAN OEDRA. Modeling the Effects of Androgens on Hormonal Regulation of the Menstrual Cycle. (Under the direction of James F Selgrade.)

Mathematical models of the hypothalamus-pituitary-ovarian axis in women were first developed by Schlosser and Selgrade in 1999, with subsequent models of Harris-Clark *et al.* (2003) and Pasteur (2011). These models produce periodic in-silico representation of Luteinizing Hormone (LH), Follicle Stimulating Hormone (FSH), Estradiol (E2), Progesterone (P4), Inhibin A (InhA), and Inhibin B (InhB). Polycystic Ovarian Syndrome (PCOS), a leading cause of cycle irregularities, is seen as primarily a hyper-androgenic disorder. Including androgens into the model is therefore necessary to produce simulations relevant to women with PCOS. As Testosterone (T) is the dominant female androgen we focus our efforts on modeling pituitary feedback and intra-ovarian follicular growth properties as functions of circulating total T levels. Optimized parameters simultaneously simulate LH, FSH, E2, P4, InhA, and InhB levels of Welt et al. (1999) and total T levels of Sinha-Hikim *et al.* (1998). The resulting model is a system of 16 ordinary differential equations, with at least one stable periodic solution. Maciel *et al.* (2004) hypothesized that retarded early follicle growth contributes to PCOS etiology. We present our investigations of this hypothesis revealing a period doubling cascade resulting in chaotic menstrual cycle behavior. Our belief that this is the first model to simulate chaotic menstrual cycles is supported by the Derry and Derry (2010) analysis of longitudinal cycle length data. We conclude this study with an investigation for biologically significant parameters m_2, t_3 and κ. Studying bifurcation diagrams of these parameters suggest a balance of pituitary feedback and follicular growth rate is necessary for successful ovulation. Hopf, saddle-node, torus, and period doubling bifurcations are examined. A unique

interval of parameters is identified for a stable periodic solution that represents irregular cycles within normal frequency that may be more representative of natural observations. A second non-ovulatory but periodic solution is presented that resembles serum hormone levels consistent with polycystic ovarian patients, often non or oligo-ovulatory. The new model may allow investigators to study possible interventions returning acyclic patients to regular cycles and guide development of individualized treatments for PCOS patients.

Modeling the Effects of Androgens on Hormonal Regulation of the Menstrual Cycle

by
Angelean Oedra Hendrix

A dissertation submitted to the Graduate Faculty of
North Carolina State University
in partial fulfillment of the
requirements for the Degree of
Doctor of Philosophy

Applied Mathematics

Raleigh, North Carolina

2013

APPROVED BY:

Claude L Hughes	Sharon Lubkin
Stephen Schecter	James F Selgrade Chair of Advisory Committee

DEDICATION

To my Family ...

To my Father ...

and to all those entrusting me to pay it forward.

BIOGRAPHY

Angelean Hendrix was raised in Port Isabel, TX. After positions in banking and broadcasting, she returned to complete her undergraduate degree in Mathematics (2007) at the University of Texas at San Antonio. Upon acceptance into the Applied Mathematics graduate program at North Carolina State University, Angelean, two daughters and husband relocated to Raleigh, NC. During her time at NCSU, Angelean was awarded a research fellowship through the National Science Foundation Graduate Research Fellowship program, completed a Master of Science in Applied Mathematics (2012) and a Doctorate of Philosophy in Applied Mathematics with a concentration in Biology (2013).

ACKNOWLEDGEMENTS

As with any journey, there are those without whom the road would be impassable. My journey began with the love and support of my friends. That first step out of the abyss found direction in numerous friends and colleagues believing in me when I could not. When the light seemed to vanish and the road to hard to bare, friends, teachers, counselors carried me through. To each and everyone that provided and still provides needs I often do not know I have, I am eternally grateful and dedicated to paying it forward.

To Barbara Knoke, who first instilled in me a love of science.

To Maribel Nawrocik, without whose inspiration, I may have never had the confidence to embark on this endeavored. You were right. Thank you for being right!

To my wonderful professors at UT-San Antonio: Ann Eisenberg, Armando Arciniega, Eduardo Dueñez, Dmitry Gokhman, Sandy Norman, Lucio Tavernini. I am fortunate to have received a world class undergraduate education, without which I could not have succeeded. To the wonderful professors Bonnie K. Lyons and Marian Aitches who taught me more about life and myself than in any of my other classes.

To all my fellow students and newfound family for the help, support, late nights and trips to "Vegas". While any attempts to name you all, would inevitably end in an unintentional omission, may I just say I have been fortunate to be surrounded by the most intelligent, strong, supportive and accepting men and women during my time at NCSU. I love each and everyone of you deeply and look forward to enjoying the lasting relationships we have formed. Though I am saddened that our time together will become increasingly infrequent, I am confident that the opportunities we do have together will seem as if no time has past. Thank you.

To Mac Law thank you for agreeing to help guide a hopeless mathematician on this

interdisciplinary road with honesty and understanding.

To Steven Schecter who taught me more about the field that has become my passion than I knew was possible. I am eternally grateful for your patience with me and belief in me.

To Sharon Lubkin for first facing the struggles that lay before me. You inspired me, encouraged me and helped me believe I could do it too.

To Mary Lou Zeeman, I can not express the wealth you have brought to my life. You sparked passion and confidence that has changed the paths of myself and my children. For continually being my mentor, advisor, friend and confidant I thank you.

To Claude Hughes who encourages unbridled enthusiasm and inquisition with enviable patience, I thank you. May our years of working together only have begun.

To James Selgrade, my advisor, my second father, and my reins. My only hope is to continually exceed your expectations and do justice to the training and inspiration you have bestowed on me.

To my father, though you are no longer with us, you live within me everyday. You were my rock, my best friend. All of the qualities I am most proud of in myself and my girls are from you.

And lastly to my family. It is easy to say you support someone's dream, it is another to work and sacrifice daily for a goal that is not your own. Everything I do is for and because of my husband and children. I have never understood why people ask me how I do what I do with a family; I don't see how I could have done any of it without you.

TABLE OF CONTENTS

LIST OF TABLES

LIST OF FIGURES

Chapter 1

Introduction

The human menstrual cycle in normally cycling women is the result of carefully balanced endocrine signaling between the hypothalamus, pituitary, and ovaries. A normal duration of 26 to 32 days is often viewed in two phases, follicular and luteal. Menstruation marks the beginning of the cycle and the follicular phase, named so for the rapid growth of ovarian follicles during this 14 day period. The follicular phase is characterized by low frequency hypothalamic gonadotropin-releasing hormone (GnRH) production that stimulates anterior pituitary synthesis and release of follicle stimulating hormone (FSH). Ovarian follicles are a central component of female reproductive physiology. Each follicle contains a single oocyte, or immature ovum, surrounded by spherical layers of specialized gonadotropin sensitive cells. Hormonally active, theca and granulosa cells, comprise the outer and inner layers of the follicle respectively. Separated by a single membrane known as the basal lamina, theca cells are the ovaries main producer of androgens while granulosa cells produce a significant portion of circulating estrogens. As the follicular phase comes to its conclusion, granulosa cells convert androgens to estrogens in response to FSH stimulation. The rise in estradiol (E2), the dominant estrogen, signals the hypothalamus

to shift to a low amplitude/high frequency GnRH secretion stimulating anterior pituitary synthesis of luteinizing hormone (LH). During the transition from follicular phase towards ovulation, unknown mechanisms determine the selection of a dominant follicle by the rapid appearance of LH receptors in the outermost layer of the follicle. Theca cells, responding to this increase in LH receptors, increase production of testosterone (T), the dominant female androgen, for conversion to E2. Simultaneously, granulosa cells increase inhibin-A (InhA) and inhibin-B (InhB) production to suppress FSH synthesis by the pituitary. At the time of ovulation, the dominant follicle can be upwards of $> 20\ mm$ in diameter, a stark contrast to its size of $< 2\ mm$ at the time of its activation. Of the ≈ 20 follicles activated in each wave, over 90% undergo atresia, or programmed cell death, with each wave of activation corresponding to a wave of atresia. As day 14 approaches, the large amounts of E2 stimulated LH releases into circulation. At this time the high frequency LH pulses produced by the pituitary in response to the high frequency GnRH pulses dramatically increase in amplitude. This interval of enhanced LH secretion is known as the LH surge. This surge in LH triggers the dominant follicle to rupture and release its ovum for possible fertilization.

Ovulation marks the beginning of the luteal phase. The follicular tissue remaining after ovulation, transforms in appearance and function to become the corpus luteum (CL). For the remainder of the cycle, the CL produces large amounts of E2, InhA, and progesterone (P4) which prevents the secretion of LH. High levels of E2 and P4 also assist in preparing the uterus for fertilization and implantation. In the event that implantation does not occur by approximately day 22, the CL begins its slow regression, transforming into a much less active corpus albicans and E2, InhA, and P4 begin to decline. This removal of ovarian hormone supported endometrial proliferation allows the onset of menstruation in preparation for the next menstrual cycle.

Mathematical studies of the hypothalamus-pituitary-ovarian axis have revealed rich and complex dynamics. In 1999, Schlosser and Selgrade developed a system of 4 delay differential equations that predicted the hypothalamically controlled pituitary synthesis and release of LH and FSH [71]. They followed this work with a compartmental model of follicular growth from which, E2, P4, and total inhibin were predicted. The two models were merged in 2003 [33] and were further expanded in 2006 to included both InhA and InhB [58]. For each model, stable periodic solutions were identified that accurately predicted serum levels of circulating reproductive hormones as reported in the literature. Analysis of the Harris-Clark merged model in 2003 also revealed an additional stable periodic solution which collaborators in reproductive endocrinology identified as consistent with the most common cause of infertility, polycystic ovarian syndrome (PCOS).

PCOS affects approximately $8-10\%$ of reproductive age females making it the most common endocrine abnormality in this population. Clinically, patients present with irregular or absent menses and elevated androgens which may result in acne, excessive hair growth, and often insulin resistance (IR) associated with increased risks of Type II diabetes and cardiovascular disease [4,27]. While heterogeneous in nature, current diagnosis standards recommend confirmation of two of the following three manifestations: 1. oligo- or anovulation, 2. hyperandrogenism, 3. visual appearance of polycystic ovaries on ultrasound. Once rare adrenal, pituitary and thyroid conditions that may present similarly to PCOS are ruled-out, treatment focuses on management of the symptoms as the etiology is not completely understood. As research begins to reveal associations between elevated androgens, IR and sub-fertility, focus has begun to shift towards classifying PCOS as a predominantly hyperandrogenic disorder. Therefore, to gain a better understanding of PCOS and the complexity of the female menstrual cycle, we focus our modeling efforts on introducing androgens into the most current model of the hypothalamus-pituitary-

ovarian axis and expanding the models representation of follicular growth and maturity.

This study presents a combination and expansion of the previous models presented by Harris-Clark [33] and Pasteur [58]. Pituitary and ovarian physiology are thoroughly reviewed as are new insights into follicular growth regulation and androgenic feedback (Chapter 2. Details of model development and mathematical theory to support this new model are subsequently discussed (Chapter 3). We follow our presentation of the model with a discussion of the current clinical data available for parameter identification, and present an estimated parameter set with methodology and statistical analysis in Chapter 4. We then present three biologically relevant bifurcations in key parameters, discussing the possible implications of the dynamics in leading to a further understanding of the underlying complexities in the etiology of PCOS. We conclude our study with a discussion of the implications of our findings and future directions for this work.

Chapter 2

Physiology

2.1 The Ovary

2.1.1 Ovarian and Follicular Physiology

The ovaries are two ovoidal organs typically located on either side of the lateral wall of the pelvis in human females. Approximately 24 cm^3, they are attached to the uterus via ovarian ligaments and are the gonadal organs in females responsible for the growth and release of ova. Research suggests that at birth, a female can have upwards of 2 million oocytes, in suspended mitosis occupying the epithelium of each ovary [31, 88]. This arrested state can be maintained for 13 to 50 years during which inactivated oocytes are surrounded by a single layer of flattened granulosa cells [88]. Histological samples of ovarian tissue reveal a complicated cellular composition that includes multiple types of stroma and connective tissue surrounding these supportive structures known as primordial follicles.

Of the original 2 million primordial follicles present at birth only 50% remain at puberty, from which approximately 20 are activated each month. The once flattened

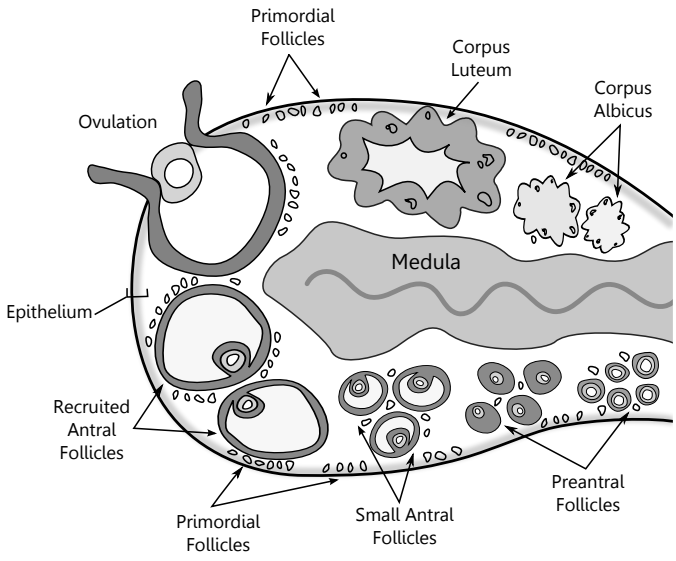

Figure 2.1: Schematic representation of ovarian mass and follicular development. Four stages of follicular maturity corresponding to previous modeling classifications are identified: Primordial, Preantral, Small Antral, and Recruited. Ovulation and CL progression is represented as well as the epithelium and medula, significant structures in this study.

granulosa cells become cuboidal and have been recently found to exhibit mRNA expression for androgen receptor (AR) [64]. As the granulosa layer multiplies, a membrane, the basal lamina forms and adjacent stroma cells differentiate in form and function to compose the follicular theca. During the first three weeks of reactivated growth, theca cells fill with lipid droplets and become highly vascularized reflecting an increase in hormonal activity [31]. Rapid growth of the granulosa layer during this period is thought to be regulated by several intra-ovarian factors including; growth differentiation factor-9 (GDF-9), kit ligand (KT), nerve growth factor (NGF), neurotrophin 4/5 (NT-4/5), brain-derived neurotrophic factor (BDNF) [54], and androgens [81]. Secondary or preantral follicles at this stage range from .025 mm to 0.150 mm in diameter [31]. Small cavities of fluid begin to appear within the granulosa cell layers that, once consolidated, form the antrum

around the maturing oocyte.

The appearance of the antrum coincides with that of FSH receptors on the surface of the granulosa cell layer [64]. As FSH sensitivity rapidly increases, all but 6-10 follicles degenerate through the programmed cell death process called atresia, while the remainder enter a recruitment phase. This developmental period coincides with the beginning of the follicular phase and the beginning of gonodotrophin stimulated growth [88]. During this fourteen day period, evidence suggests FSH must rise above a threshold level for five days during which a select subgroup of small antral follicles experience rapid growth. This time in the menstrual cycle is referred to as the FSH window [23]. Recruited follicles can grow from 2 mm to approximately 15 mm in diameter during this time [31]. Circulating FSH stimulates aromatase conversion of androgens to estrogens within the granulosa cells [31] to E2. As the recruitment period concludes, FSH begins to decline and a single follicle is selected from this cohort by its acquisition of LH receptors for impending ovulation. The dominant follicle can grow up to 20 mm in diameter. Remaining follicles succumb to atresia without the necessary receptors to shift to LH dependent growth. Just prior to mid cycle, the increased androgen production facilitates increased secretion of E2, promoting pituitary LH production. On approximately day 14, the ever increasing stores of synthesized LH are released into circulation. The resulting LH surge initiates localized lysis in the follicular wall allowing the extrusion of the oocyte, now competent for fertilization, to travel towards the fallopian tubes [54, 88].

Transition towards the luteal phase of the cycle coincides with a dramatic transformation of the tissue remaining after ovulation. Referred to as the corpus luteum (CL), the tissue develops a yellow appearance and rapidly increases in mass. Its production of high levels of E2, P4 and InhA regulate luteal phase pituitary hormone synthesis through their influence on GnRH amplitude and frequency. Luteal ovarian steroid production

peaks approximately 7 days after ovulation. In the absence of pregnancy, the CL begins its regression, declining in size and activity during the remainder of the menstrual cycle. Now hormonally quiescent, the CL becomes a corpus albicans and slowly declines in mass as the subsequent cycle begins [54, 88].

2.1.2 Ovarian Mass

Each follicular development/atresia cycle is often viewed as a discrete event, however, histological studies, reveal numerous follicles of diverse sizes from 1 mm to 20 mm in diameter during most of the menstrual cycle [31]. As current ultrasound technology is best at identifying follicles greater than 2 mm [36], it is common to consider this as the point of primary follicle activation. Waves of follicular activation have been recently documented by Baerwald *et al.* [6]. In their study each wave of follicular activation coincides with an atretic wave of older follicles. A slight elevation in ovarian mass can be observed with the appearance of the dominant follicle [41] with the peak in ovarian mass occurring at approximately day 19 of the cycle [41] due to CL development. In normal ovaries, total ovarian mass remains within $\pm 10\%$. Extended estrogen-based contraception and reproductive disorders like PCOS can affect the average size of each ovary over months years, but have not been shown to be significantly related to fluctuations in mass within a single cycle. These findings supports the possibility of a signaling mechanism that maintains a total ovarian mass steady state. At this time, extra-ovarian endocrine regulation preventing unbounded ovarian mass has not been identified. Local factors identified during follicular fluid analysis are commonly accepted as major contributors in this regulation. It is hypothesized that follicles in a more advanced growth stage regulate activation of a new wave of follicles through the use of insulin like growth

factors [43], transforming growth factor ($TGF\beta 1$) [39], granulosa-theca cell factors [55], anti-Müllerian hormone [77], and androgens [64]. While, follicular fluid content of growth factors significantly affects ovarian mass and follicular maturation, these factors are difficult to quantify in serum. Furthermore, as our goal is to further understand clinically accessible markers relating to PCOS etiology, modeling relatively inaccessible follicular fluid content transcends our current scope.

2.1.3 Androgenic Follicular Growth Regulation

Alterations in the ovarian follicular growth cycle have been implicated in investigations of cycle irregularities and infertility. Studies of women with PCOS report stockpiling of follicles with diameters $\leq 0.2\ mm$ [44] and unregulated follicle growth [20]. Elevated serum androgens are a common endocrine feature of PCOS and animal models suggest these androgens may contribute to its etiology [28, 32, 83, 90]. The most common of these androgens implicated in PCOS is T, the classical male hormone that is elevated in a significant portion of patients with PCOS [2, 65]. AR have been found in all follicular cell types, including oocytes. AR-knockout mice display increased granulosa cell apoptosis, a decreased number of antral follicles, are subfertile, have fewer CL and ovulate less frequently than normal mice [72]. Women exposed to exogenous androgens, as seen in gender reassignment studies and in women with congenital adrenal hyperplasia, are observed to have enlarged ovaries, theca-interna hyperplasia, and an increased number of large "cystic" follicles [29, 56, 76]. This morphology is consistent with that of many PCOS women, raising the possibility of gender reassignment patients serving as a human model of the disorder [56]. Studies of theca cells from classical PCOS patients suggest an abnormality in local insulin receptor dynamics of larger antral follicles, where stimulation

results in up to a four fold increase in T production [51]. This becomes problematic as granulosa cells of developing follicles as small as 0.2 mm stain positive for AR [64]. While not completely understood, these findings call for a further understanding of intra-ovarian androgen signalling as a possible component in PCOS etiology.

2.2 Hypothalamus and Pituitary

2.2.1 Physiology

The pituitary is a lobular gland connected to the base of the hypothalamus that is divided into three distinct lobes: anterior, intermediate, and posterior [31, 54, 88]. Hypothalamic control of gonadotrophin synthesis and release is well established [88], and there are both direct and indirect feedback loops within the hypothalamic-pituitary-ovarian axis. Pituitary receptors for ovarian hormones estrogens, progestogens and androgens are found in highest concentration in the gonadotroph cells of the anterior lobe [79]. Responsible for reproductive endocrine activity, the gonadotrophs comprise 7% to 15% of all anterior pituitary cells. Immunohistochemical studies indicate positive staining for both LH and FSH in approximately 70% of gonadotrophs, suggesting that each cell is capable of synthesizing LH and FSH contingent on GnRH stimulatory patterns. It has been found that GnRH pulse frequency is positively correlated with mean LH levels, while inversely related to serum FSH [88].

Knobil and colleagues first documented this complicated relationship in rhesus monkeys with hypothalamic lesions. Their further studies laid the foundation for much of what we know about ovarian steroid feedback on both the hypothalamus and pituitary (see Figure 2.3). In 1982, the Knobil lab was the first to suggest a bi-phasic response

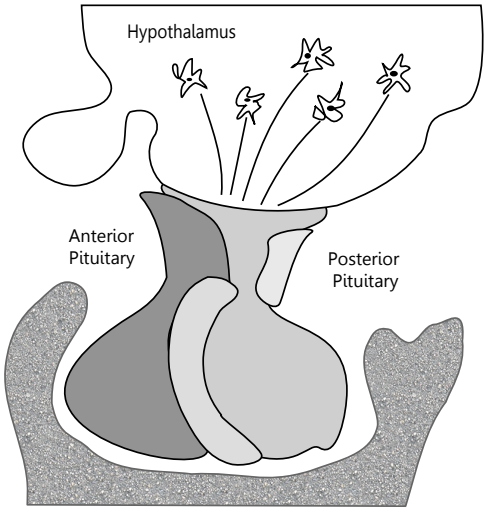

Figure 2.2: Diagram of hypothalamus-pituitary physiology noting the location of the hypothalamus, anterior pituitary, and posterior pituitary.

of gonadotropins to serum E2 [35]. Estrogen responsive GABA neurons are thought to play a major role in negative feedback of E2 within the preoptic area of the hypothalamus. In postmenopausal and ovariectomized women, low doses of E2 administration are well known to inhibit gonadotropin secretion [88]. The negative effects of E2 on LH are believed to be predominantly secondary to the inhibition of GnRH, while preovulatory positive E2 feedback is considered to be through direct stimulation of estrogen receptors in the pituitary which in turn increases GnRH receptor numbers [88]. P4 has been demonstrated to inhibit both glslh and FSH via the beta-endorphin system at the hypothalamus level. It is hypothesized that a significant proportion of the negative feedback of E2 is through up-regulation of the progesterone receptor [31,79,88]. Further negative feedback, specifically on pituitary FSH, can be observed in inhibin-sensitive gonadotrophs, where it is believed they interfere with GnRH mediated baseline synthesis.

2.2.2 Androgenic Pituitary Feedback

Recently much attention has been focused on investigations of androgen feedback on the pituitary, as elevated levels significantly correlate with reproductive cycle disruption found in patients with PCOS [3, 13, 27]. In human females elevated T is significantly correlated with elevated basal LH levels and diminished LH surge [24, 80]. Immunohistochemical staining has localized AR in rat and human female anterior pituitary sections in concentrations similar to those in males [68, 79]. This finding suggests a direct role of androgens in controlling gonadotroph LH synthesis. Studies also suggest the role of androgens at the pituitary level is to prime gonadotrophs for GnRH activation through its facilitation of LHβ mRNA expression [87]. The androgens T and DHT in females have both been found to affect positively gonadotroph synthesis of LH. As T (but not DHT) is a precursor to E2, the positive effect of both androgens is independent of T's conversion to E2 [87]. In rat pituitary cells pituitary feedback has also been shown to occur through T's increase of GABAergic transmission to GnRH neurons [60]. Additionally, isolated rat GnRH neurons have been shown to display increase pulse frequency in the presense of T, that would suggest a possible mode of action that could increase the LH synthesis response [49]. The role of androgens is further supported in clinical studies of flutamide treatment in PCOS patients. Flutamide, an androgen receptor blocker has shown promising results in restoring cyclicity in anovulatory patients during long term clinical trials [16, 18].

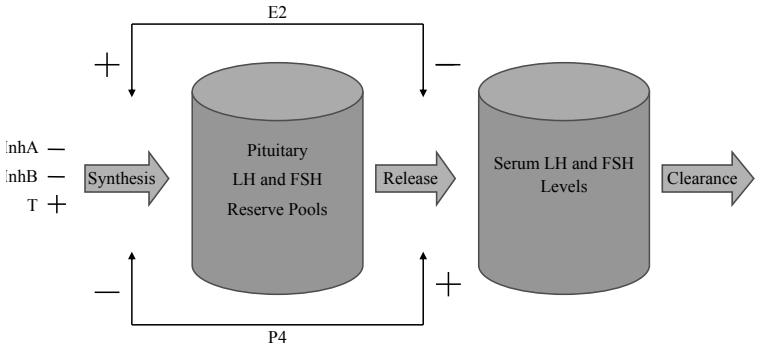

Figure 2.3: Ovarian control of the GnRH modulated pituitary synthesis and release of LH and FSH. Stimulatory and inhibitory effects are denoted by + and - signs, respectively.

Chapter 3

Model Development

Previous models for hormonal regulation of the menstrual cycle have been constructed using systems of ordinary differential equations where state variables represent serum hormone levels or different stages of monthly ovarian development, e.g., Harris-Clark *et al.*, 2003 [33], Reinecke and Deuflhard, 2007 [63], and Pasteur and Selgrade, 2011 [59]. The model presented here expands on the models of Harris-Clark *et al.* [33] and Pasteur and Selgrade [59] by expanding representation of follicular growth regulation and including the effects of the androgen T on the brain and ovaries.

The development of the follicle which releases its ovum in a specific menstrual cycle begins at least 60 days before that cycle [52]. Abnormal development during this period of early growth may result in cycle irregularities consistent with PCOS [1, 5, 77, 88]. In fact, Maciel *et al.* [44] reported a "stockpiling" of preantral follicles in women with PCOS as compared to normally cycling women. While the development of preantral follicles is gonadotropin independent, intra-ovarian factors [44, 62, 75] influence the early growth and transition to the antral stage. Androgen receptors have been shown to appear on follicles during the earliest stages of maturity, before gonadotropin receptors [64]. In

this study we consider the effects of T and intra-ovarian factors on preantral and early antral follicles and its positive feedback on the pituitary by presenting an expansion of the Harris-Clark [33] and Pasteur [58] models that reflects the latest findings in early follicular development and androgenic pituitary feedback.

3.1 Ovarian Modeling Technique

3.1.1 Foundation

Early attempts in modeling preovulatory follicular growth under the previous compartmental model approach revealed deficiency in the ability to model simultaneous growth among stages. As our goal includes intra-ovarian influence for the first time we first had to identify an appropriate method to represent this relationship. We begin by dividing the follicular growth and regression process into 12 stages of maturity; $PrA1$ (preantral follicle 1), $PrA2$ (preantral follicle 2), $SmAn$ (small antral follicle), RcF (recruited follicles), OvF (ovulatory follicle), $CLi : i = 1 \ldots 2$ (corpus luteal development), and $Luti : i = 1 \ldots 4$ (luteal phase). Stage specific receptor dynamics are schematically represented in figure 3.1, with positive and negative influence identified by $+$ and $-$ respectively. Using existing equations for OvF through $Lut4$, we focus our attention on the dynamics of preovulatory growth within a bounded system. Mathematical theories of mass action kinetics, often used in chemistry, presented a possible approach to this challenge. Used to describe chemical reactions where the total mass or volume of a system remains constant while the individual components change dynamically, the mass action approach allows us to reflect total mass steady state regulation while reflecting the individual shifts in mass through maturity stages. The corresponding model equations are

built to reflect this interdependent shift of mass through three stages of maturity, pre-antral 1 and 2, and small antral, with state variables $PrA1$, $PrA2$, and $SmAn$. This approach captures the intra-ovarian effects on early follicular development reviewed in section 2.1.1.

Observations suggest primordial follicles migrate from the epithelium to the medula upon activation, and return to the epithelial layer as maturation progresses [25]. This implies that any intra-ovarian signaling may be spatially determined and correlate with maturity level. Transitions through these stages, therefore, depend on the masses of adjacent stages and available hormone levels. We assume that proximity between follicles determines the magnitude of interfollicular signaling with the most significant effects coming from the subsequent maturity levels as the follicles migrate towards the outer cortex of the ovary. This allows us to emulate intra-ovarian signaling when follicular fluid levels of growth factors cannot be quantified.

3.1.2 Quantifying Follicular Development

We begin our modeling attempts at the point of reactivated mitosis with our first equation for preantral follicle growth. The growth term in our first stage, $PrA1$, has a constant rate, m_1, of primordial follicle recruitment as suggested by Gougeon [31]. We introduce a T dependent transfer term that scales the product of the current mass ($PrA1$) with the mass of the next stage of maturity ($PrA2$). This term reflects the appearance of androgen receptors before gonadotropin growth begins [64] and contains an exponential, η, introduced to control the rate of stimulatory response to T . The equation for $PrA1$ becomes:

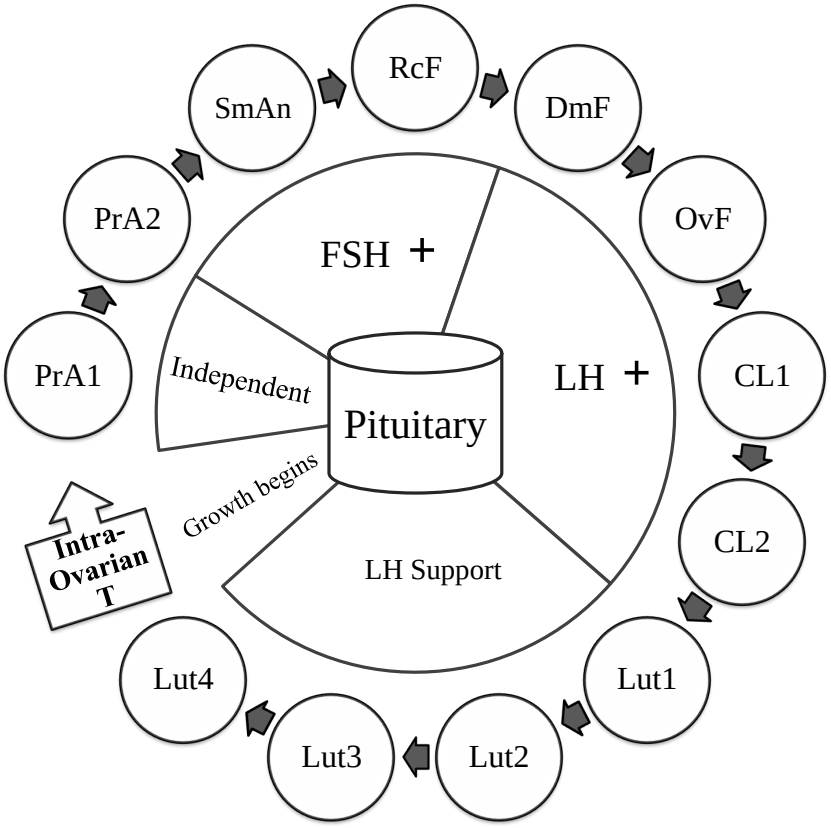

Figure 3.1: State variables representing 12 stages of follicular development are shown. Follicle growth begins with the $PrA1$ stage and continues in a clockwise direction for a complete cycle. The pie chart indicates the timing of the regulatory effects of luteinizing hormone (LH) and follicle stimulating hormone (FSH) on follicular development.

$$\frac{d}{dt}PrA1 = m_1 - m_2 \cdot T^{\eta} \cdot PrA1 \cdot PrA2 \tag{3.1}$$

In this equation, our introduction of T coincides with the time at which AR are found on the granulosa cells of the follicles. The product term $PrA1 \cdot PrA2$ prevents both stages from growing simultaneously, given the assumption that an increased mass

in $PrA2$ must be a result of a diminishing mass of $PrA1$ maturity stage follicles. This product also quantifies the intra-ovarian growth factor influence from the most adjacent neighbor. Consistent with models of this type, our transfer term

$$m_2 \cdot T^{\eta} \cdot PrA1 \cdot PrA2$$

becomes the growth term for our next stage of maturity $PrA2$.

As reviewed in chapter 2.1.1, FSH receptors are the next to be found on granulosa cells once the antrum begins to develop. We use this fact to shift our mass from $PrA2$ utilizing an FSH dependent threshold term (e.g., see Zeleznik [89])

$$m_3 \cdot \frac{FSH^{\nu}}{Km_{FSH}^{\nu} + FSH^{\nu}} \cdot$$

This gradual acquisition of receptors and saturation behavior is translated mathematically through a Hill function whose product with the current stage, $PrA2$, and following stage, $SmAn$, again allows us to represent intra-ovarian factors.

$$\frac{d}{dt}PrA2 = m_2 \cdot T^{\eta} \cdot PrA1 \cdot PrA2 - m_3 \cdot \frac{FSH^{\nu}}{Km_{FSH}^{\nu} + FSH^{\nu}} \cdot PrA2 \cdot SmAn \qquad (3.2)$$

As the mass of $PrA2$ is dependent on that of $SmAn$, there exists an indirect effect of $SmAn$ on our first stage, $PrA1$. This assumes that migration, from the medula region, increases the distance from $SmAn$ follicles to the $PrA1$ follicles and, therefore, the inter-follicular signaling between the two decreases. The last stage of mass action dependence,

$SmAn$, provides the small antral follicle mass available for recruitment whose growth is partially regulated by follicles in $PrA2$, and indirectly by follicles in $PrA1$ through its inclusion in the equation for $PrA2$.

$$\frac{d}{dt}SmAn = m_3 \cdot \frac{FSH^{\nu}}{Km_{FSH}^{\nu} + FSH^{\nu}} \cdot PrA2 \cdot SmAn - b \cdot FSH^{g} \cdot SmAn \cdot RcF \qquad (3.3)$$

For the decay term we assume that the rate of FSH receptor acquisition rapidly increases to a point directly proportional to the natural rise in follicular phase FSH at the beginning of the follicular phase [31], rather than a threshold response used in the previous stage. Similarly, the transfer of mass from $SmAn$ is affected by the existing mass in the subsequent stage RcF whose growth is affected by $SmAn$ directly (see eq. 3.3) and by $PrA1$ and $PrA2$ indirectly (see eqs. 3.2, 3.1).

To reflect the increasing ovarian mass as we approach ovulation and the luteal phase of the cycle, linear growth and decay terms are employed in 9 different stages which represent ovarian development as originally presented in Schlosser and Selgrade [69]. RcF represents recruited follicles available to respond to the impending FSH window and therefore necessitates an additional FSH dependent growth term. The compartmental portion of our model permits total ovarian mass to increase as the ovaries approach the time at which a dominant follicle is selected. DmF and OvF represent the dominant and ovulatory follicle. $CL1$ and $CL2$ portray the transition to the corpus luteum. The luteal phase consists of the four stages $Luti : i = 1 \ldots 4$ representing the regression of the CL and conclusion of the current monthly cycle (Figure 3.1). These 9 stages correspond to

the ovarian model of Harris-Clark *et al.* [33], with growth and decay terms as indicated in the following differential equations:

$$\frac{d}{dt}RcF = b \cdot FSH^{\varrho} \cdot SmAn \cdot RcF + (c_1 \cdot FSH - c_2 \cdot LH^{\alpha}) \cdot RcF \tag{3.4}$$

$$\frac{d}{dt}DmF = c_2 \cdot LH^{\alpha} \cdot RcF + (c_3 \cdot LH^{\beta} - c_4 \cdot LH^{\xi}) \cdot DmF \tag{3.5}$$

$$\frac{d}{dt}OvF = c_4 \cdot LH^{\xi} \cdot DmF - c_5 \cdot LH^{\gamma} \cdot OvF \tag{3.6}$$

$$\frac{d}{dt}CL1 = c_5 \cdot LH^{\gamma} \cdot OvF - d_1 \cdot CL1 \tag{3.7}$$

$$\frac{d}{dt}CL2 = d_1 \cdot CL1 - d_2 \cdot CL2 \tag{3.8}$$

$$\frac{d}{dt}Lut1 = d_2 \cdot CL2 - k_1 \cdot Lut1 \tag{3.9}$$

$$\frac{d}{dt}Lut2 = k_1 \cdot Lut1 - k_2 \cdot Lut2 \tag{3.10}$$

$$\frac{d}{dt}Lut3 = k_2 \cdot Lut2 - k_3 \cdot Lut3 \tag{3.11}$$

$$\frac{d}{dt}Lut4 = k_3 \cdot Lut3 - k_4 \cdot Lut4 \tag{3.12}$$

3.1.3 Serum Hormones

Follicular growth and hormonal clearance rates can exist on very different time scales. In our study, changes in follicular development and hormonal activity are best understood over days, while total body clearance for the hormones produced by the ovaries occurs over minutes and hours [8]. This allows us to assume that circulating levels of the ovarian hormones are maintained at a quasi-steady state as in Bogumil *et al.* [12] and is thoroughly reviewed in Keener and Sneyd [37]. Implementation of this approach allows us to

estimate serum levels of ovarian hormones as linear combinations of the active follicular mass at the time of production. In our case, linear combinations of the 12 ovarian stages (see eqs. 3.1 - 3.12) result in the following four auxiliary equations for serum $E2$, $P4$, $InhA$, and $InhB$:

Auxiliary Equations (A)

$$E2 = e_0 + e_1 \cdot DmF + e_2 \cdot Lut4 \tag{A1}$$

$$P4 = p_1 \cdot Lut3 + p_2 \cdot Lut4 \tag{A2}$$

$$InhA = h_0 + h_1 \cdot OvF + h_2 \cdot Lut2 + h_3 \cdot Lut3 \tag{A3}$$

$$InhB = j_1 + j_2 \cdot PrA2 + j_3 \cdot SmAn + j_4 \cdot RcF + j_5 \cdot CL1^{j_6} \tag{A4}$$

To construct the equation for circulating T, we began with a linear combination of the ovarian stages (see eq: 3.2 - 3.12) as no evidence exists to support hormonal activity during our first stage of development ($PrA1$). Parameter fitting to data, as covered in detail in section 4.3, reveals little to no synthesis of T from the ovarian stages $CL1$, $Cl2$, $Lut2$, and $Lut4$. The final equation for circulating T becomes:

$$\begin{aligned} T = {} & t_1 + t_2 \cdot PrA2 + t_3 \cdot SmAn + t_4 \cdot RcF + t_5 \cdot DmF \\ & + t_6 \cdot OvF + t_7 \cdot Lut1 + t_8 \cdot Lut3. \end{aligned} \tag{A5}$$

3.2 Hypothalamus-Pituitary Model

GnRH produced by the hypothalamus, on a time scale of minutes and hours, stimulates pituitary gonadotroph synthesis of LH at higher pulse frequencies and FSH at lower pulse frequencies [11]. Original modeling efforts by Schlosser and Selgrade (2000) [69] combined the ovarian hormone stimulation of both the hypothalamus and the pituitary in a system of four differential equations for the synthesis, release and clearance of the gonadotropin hormones. This coupling of hypothalamus and pituitary action allows the system to predict gonadotropin levels on a time scale consistent with published clinical data (McLachlan *et al.* [47] and Welt *et al.* [84]). Moreover, their model utilizes findings that the pituitary-ovarian feedback loop responds to average daily blood levels [53]. It therefore becomes advantageous for our purposes to track the average daily serum concentrations of FSH and LH as a reflection of overall hypothalamic-pituitary function.

3.2.1 Quantifying Gonadotropin Synthesis and Release

State variables RP_{LH} and RP_{FSH} represent the amounts of synthesized hormones in the pituitary via GnRH signaling; LH and FSH represent the blood concentrations of these hormones. To begin, a baseline synthesis rate is assumed to be constant for both hormones. This is reflected with the constant terms v_0 and v_{FSH} in both equations RP_{LH} and RP_{FSH}. Through changes in GnRH pulse frequency and amplitude, LH exhibits a biphasic response to E2 [42], so to account for this the model assumes that the effect of E2 on LH synthesis is different than the effect on LH release. To model this relationship, the denominator of the second term for RP_{LH} (see eq. 3.13) reflects E2's inhibition of LH secretion, while at high levels E2 promotes LH synthesis in a dose dependent fashion by the utilization of a Hill function in the numerator of our equation for RP_{LH} (see eq.

3.13). The effect of P4 on GnRH modulated LH and FSH synthesis are inhibitory, while P4 has been shown to promote LH release from the pituitary. Our P4 term appears in the denominator of our synthesis term and in the numerator of both release terms for LH and FSH (see eqs. 3.13 and 3.16). For FSH synthesis, a constant production is assumed which is down regulated by InhA and InhB (see eq. 3.16). Discrete time-delays, d_E, d_P, d_{InhA} and d_{InhB}, were assumed for the effects of E2, P4, InhA and InhB on gonadotropin synthesis to reflect the underlying biochemical process involved in hormone synthesis.

Circulating levels of FSH and LH, as measured clinically, will depend on three factors: 1) synthesized quantities of each hormone, 2) blood volume, 3) whole body clearance rates. Our equations for serum levels therefore become functions of the release terms from each reserve pool equation, scaled by average blood volume v, and clearance rates r_{LH} and r_{FSH} derived from literature [14, 38] (see eqs. 3.16 and 3.14).

In our attempt to reflect androgenic feedback actions of T on the pituitary, reviewed in 2.2.2, we remind the reader that androgens have been found to modulate GnRH LH synthesis independent of aromatase conversion to E2. To that end, we construct the term with time delay d_T and exponent κ to allow us to manipulate the timing and response rate to T. The original model of Schlosser and Selgrade [69] assumed a baseline LH synthesis rate v_0 independent of E2. Motivated by Yasin *et al.* [87], our model assumes that this baseline rate, v_0, depends on $T(t-d_T)^\kappa$, see eq. 3.13 becoming the introduction point for reflecting androgenic feedback. The revised equations for our pituitary states variables are detailed in equations 3.13 through 3.16.

$$\begin{aligned}\frac{d}{dt}RP_{LH} &= \frac{v_0 \cdot T(t-d_T)^{\kappa} + v_1 \cdot \dfrac{E2(t-d_E)^a}{(Km_{LH}^a + E2(t-d_E)^a)}}{\left(1 + \dfrac{P4(t-d_P)}{Ki_{LH}}\right)} \\ &- k_{LH} \cdot \frac{\left(1 + c_{LHp} \cdot P4^{\delta}\right)}{(1 + c_{LHe} \cdot E2)} \cdot RP_{LH}\end{aligned} \tag{3.13}$$

$$\frac{d}{dt}LH = \frac{1}{v} \cdot k_{LH} \cdot \frac{\left(1 + c_{LHp} \cdot P4^{\delta}\right)}{(1 + c_{LHe} \cdot E2)} \cdot RP_{LH} - r_{LH} \cdot LH \tag{3.14}$$

$$\begin{aligned}\frac{d}{dt}RP_{FSH} &= \frac{v_{FSH}}{1 + \left(\dfrac{InhA(t-d_{InhA})}{Ki_{FSHa}}\right) + \left(\dfrac{InhB(t-d_{InhB})}{Ki_{FSHb}}\right)} \\ &- k_{FSH} \cdot \frac{(1 + c_{FSHp} \cdot P4)}{(1 + c_{FSHe} \cdot E2^{\zeta})} \cdot RP_{FSH}\end{aligned} \tag{3.15}$$

$$\frac{d}{dt}FSH = \frac{1}{v} \cdot k_{FSH} \cdot \frac{(1 + c_{FSHp} \cdot P4)}{(1 + c_{FSHe} \cdot E2^{\zeta})} \cdot RP_{FSH} - r_{FSH} \cdot FSH \tag{3.16}$$

Chapter 4

Parameter Identification and Statistical Analysis

4.1 Formulating a Statistical Model

Modeling biological systems, especially in humans, can present unique challenges. Of the 70 parameters used to develop our model three are currently identifiable in the literature.

- v: average blood volume in liters
- r_{FSH}: metabolic clearance rate of FSH
- r_{LH}: metabolic clearance rate for LH

For the remaining parameters the challenge then becomes to find a solution to the associated inverse problem using parameter estimation techniques. Additionally one must consider the certain degree of error intrinsic in any biological measurement. In our case, the data available for parameter estimation can be assumed to be further perturbed through the data extraction process as well as natural variability. While the focus of this

model prioritizes qualitative agreement, this magnification presents challenges when estimating the remaining parameters and determining the effectiveness of these estimates. To investigate this issue we first look at the intrinsic statistical model that results from the assumption that the biological dynamics can be captured mathematically. A statistical model of the form:

$$\Phi(t_i) = \Psi(t_i; \theta) + \bar{\varepsilon}_i. \tag{4.1}$$

is generated such that i reminds the reader of variation in error between each time measurement. In this model Φ represents the quantified biological dynamics, Ψ is the mathematical model of this behavior, $\theta \in \mathbb{R}^n$ is our unknown "true" parameter vector, and $\bar{\varepsilon}$ represents the intrinsic measurement error. At this point we assume that our measurement errors, ε_i, are independent, identically distributed (IID) random variables with zero-mean and constant variance. Furthermore, as θ is unknown, Ψ becomes:

$$\Psi(t_i; \theta) = \Psi(t_i; \hat{\theta}) + \hat{\varepsilon}_i, \tag{4.2}$$

such that $\hat{\theta} \in \mathbb{R}^n$ denotes the estimates for parameters that are not experimentally verifiable, and $\hat{\varepsilon}_i$ quantifies errors occurring through the estimation process. If we assume that this error too is IID, we can combine both measurement and estimation error into a single vector ε and analyze the resulting statistical model

$$\Phi(t_i) = \Psi(t_i; \hat{\theta}) + \varepsilon_i. \tag{4.3}$$

This equation provides a closed form measurement for our residual for use in parameter estimation. Further assumption that the underlying model dynamics are continuously

differentiable allows us to invoke standard non-linear regression approximation theory to investigate the sampling distribution for the resulting $\hat{\theta}$ [22, 26]. First though, we must examine the available data and determine $\hat{\theta}$.

4.2 Clinical Data

The preceding model of Pasteur [58] utilized daily serum levels as reported by Welt *et al.* [84]. This data set, detailed in Appendix A.2 Table 5, provides mean daily serum hormone levels for LH, FSH, E2, P4, InhA, and InhB. The Welt *et al.* study included 23 normally cycling women between the ages of 20 and 34 [84]. For our purposes it became necessary to identify a similar data set that included serum T for normally cycling women. While data sets that meet our criteria may exist, a thorough literature search on PubMed did not identify a suitable published data set. We were able to identify serum T levels for 37 normally cycling women between the ages of 20 and 45 in a study by Sinha-Hikim *et al.* [73]. Their study presented mean serum levels for 9 days over an average cycle, 4 follicular phase, 1 at ovulation, and 4 during the luteal phase that were extracted from the literature using the graphical digitizing software DigitizeIt © [1]. To construct a complete data set that was sufficient for our purposes, linear extrapolation via MATLAB's *interp* function [46] was used to generate 28 days of serum T data. For comparison purposes we converted the Sinha-Hikim data from nmol/L to ng/dL. This conversion (see Appendix A.4) takes the range of values from $(.7, 1.6)$ to $(20, 47)$. This becomes mathematically advantageous as it allows our simulated values to remain strictly greater than 1. The resulting vector combined with the data of Welt *et al.* [84] composed the clinical data matrix used for parameter estimation, detailed in Appendix A.1 Table 5 and represented

[1] Copyright 2008, Digitize It Now, Inc. All rights reserved

in Figure 4.1.

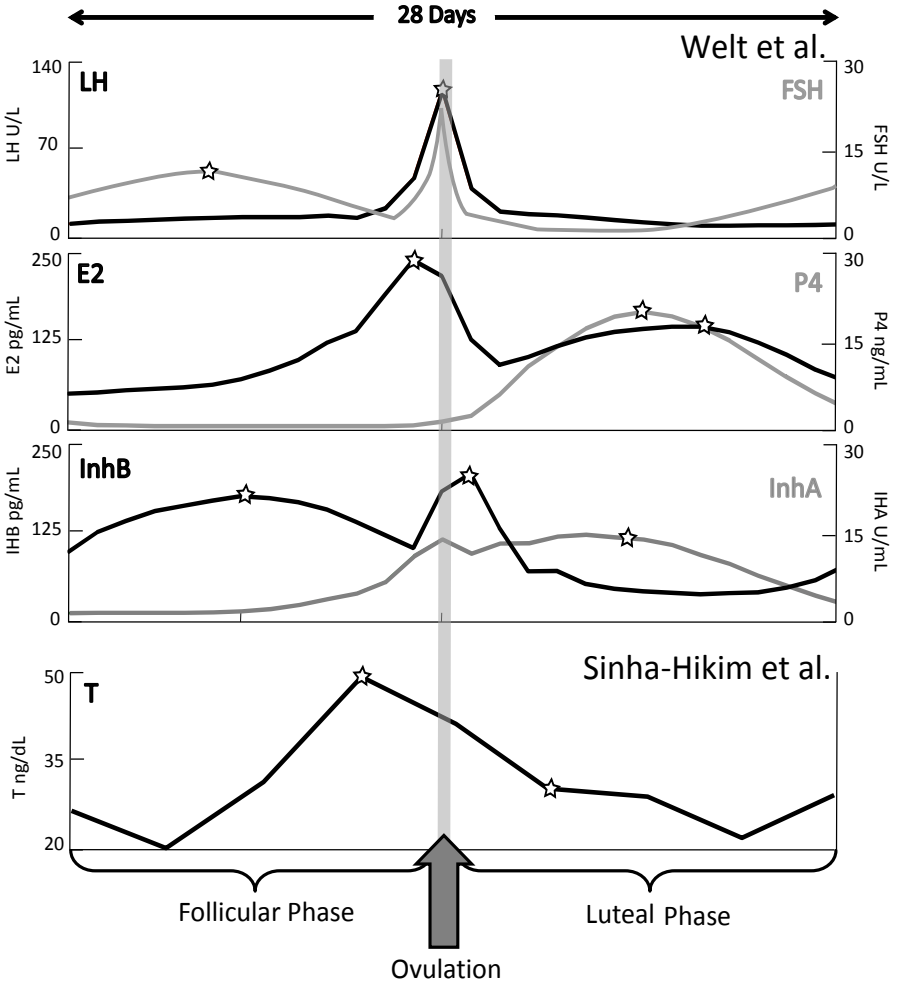

Figure 4.1: Clinical data as extracted from Welt *et al.* and Sinha-Hikim *et al.* Data points of greatest biological significance designated by $\star$

4.3 Parameter Estimation

One object of this study is to predict serum levels of circulating endocrine hormones for use in *in-silico* experimentation. To this end it becomes necessary to identify biologically consistent parameters for the model described in Chapter 3.

To begin we first formulate an initial set of parameters that reasonably produce predictions within $\pm 30\%$ of the mean serum levels of existing data sets for each hormone. This initial parameter vector, $\hat{\theta}_I \in \Re^n$, consists of the previously identified parameters for the ovarian compartmental equations as reported in Harris-Clark *et al.* [33] and the pituitary and auxiliary parameters from Pasteur 2008 [58]. The remaining parameters were initially estimated with a manual ad hoc technique that focused on parameters for equations 3.1 through 3.4, as the stability of this portion of the system is of the utmost importance.

For our inverse algorithm we initially employ a Nelder-Mead direct approach via MATLAB's *fminsearch* function [46]. This approach was chosen, not only for its simplicity, but for its effectiveness in identifying a global minimum, an obstacle using available gradient method packages in our particular circumstances. To ensure our parameters remain positive and therefore biologically relevant, we implement our algorithm on the *log* transform of our parameter space. The Nelder-Mead approach attempts to minimize the difference, or "cost", between the model predictions and clinical data.

The traditional least squares function of residuals returned an appropriate initial cost function:

$$Cost_I = \sum_{j=1}^{7} \sum_{i=1}^{28} \left(\frac{y_{i,j}}{D_j} - \frac{\Psi_{i,j}}{D_j} \right)^2 . \tag{4.4}$$

We note here that our clinical data is reported daily, with a total of 28 data points per hormone. Our solution output is evaluated at a frequency of .1 time steps per day. To reconcile this inconsistency, we find it appropriate to sample our solution daily to remain consistent with the data. To distinguish between the two, natural vectors of daily values will be denoted using i as indices and $\hat{i}$ will be used to inform the reader should the full solution vector be utilized. For our cost function, j denotes the 7 hormones predicted, D_j is the mean for each reported hormone level across the cycle, $y_{i,j}$ is our matrix of clinical data, and $\Psi_{i,j}$ is our sampled solution matrix.

Within our context, the number of parameters ($n = 70$) can be considered large when compared to the number of data points available for estimation. This presents risks of over-parameterization, ill-conditioning and the possibility of sacrificing important qualitative behavior given the variations in output scales. Moreover, outputs of low biological significance, low amplitude variations in LH during the luteal-follicular phase transition for example, can skew the focus from the points of greatest concern. To address these issues, 2 methods were utilized in constructing additional cost functions: weighted least squares and non-random re-sampling.

Optimizations were maximized at 1000 iterations per run. Using our traditional least squares function, $Cost_I$ (see equation 4.4), goodness of fit was assessed qualitatively after each optimization run. It become apparent that for our periodic solution, outputs with large means and range in oscillations dominated the optimization protocol through their increased contribution to the overall cost. To overcome this challenge, weights were assigned to increase the effect of lower amplitude oscillatory outputs on the cost function that held the most biological significance. Qualitative analysis for each $\Psi_{:,j}$ vs. $\Phi_{:,j}$ proved to be the most accurate and efficient means of identifying the location and magnitude of each weight. Early attempts at multiple weights produced less than satisfactory results

leading to the use of a single weight per optimization run using the following weighted cost function:

$$Cost_W = \sum_{j=1}^{7} \left[w_j \cdot \sum_{i=1}^{28} \left(\frac{y_{i,j}}{D_j} - \frac{\Psi_{i,j}}{D_j} \right)^2 \right]. \tag{4.5}$$

where w_j represents the aforementioned weight assigned to the appropriately determined output j. For each application of the Nelder-Mead algorithm, a $\hat{\theta}_k$ was identified, with k used as a counter for the iterative application. Relative changes,

$$RC_k = \frac{|\hat{\theta}_k - \hat{\theta}_{k+1}|}{|\hat{\theta}_k|}, \tag{4.6}$$

were calculated between each run for use in identifying which subset $\hat{\theta}_s \in \hat{\theta}_k$ experienced the greatest adjustment during minimization of the weighted cost. Many times sorting RC_n by amplitude revealed a sharp decline in values that determined the number of parameters in $\hat{\theta}_s$. At times a natural cut off point was not apparent, the subset $\hat{\theta}_s$ was defaulted to 10 values. For run $k+2$ we reutilize the weighted cost function from equation 4.5, fixing $\hat{\theta}_{k+1}|_{\hat{\theta}_s}$ within $\hat{\theta}_{k+1}$ and proceed until the net change in the residual between iterations met a tolerance level of 10^{-2}.

This approach accomplished two important goals:

1. Overcoming the dominance of cost measurements for outputs of high oscillation
2. Allowing qualitative influence on the cost calculation

Unfortunately due to the natural fluctuation seen in the clinical data, this approach fell short in capturing all of the most biologically significant behavior simultaneously. Furthermore, the repeated application of a computationally expensive algorithm proved inefficient.

Recently, much attention has been focused on the benefits of "Bootstrapping" in parameter estimation. Bootstrapping is a statistical method that alternates the cost function between optimization runs by measuring the residual against a subset of data randomly sampled with replacement. After each iteration, goodness of fit is measured, and the parameter set that generates a solution with the least residual across the entire data set is used for the following iteration [19]. If we look at our clinical data (see Figure 4.1), we can see that a random sampling approach may only capture data during times of little dynamical change. Focused resampling of our data during optimization has the opportunity to ensure the most significant biological behavior is captured. Ten points of greatest significance were identified: LH surge levels, FSH mid follicular crest, E2 preovulatory surge and mid-luteal crest, P4 crest, InhA peak and luteal crest, InhB mid-follicular crest, T preovulatory elevation and descent (see Figure 4.1). The times associated with these events were used to generate a time sequence $i*$ for sampling purposes. The resulting subset of clinical data is used to formulate a further variation of least squares with the aforementioned weights to obtain:

$$Cost_{WS} = \sum_{j=1}^{7} \left[w_j \cdot \sum_{i*=1}^{10} \left(\frac{y_{i*,j}}{D_j} - \frac{\Psi_{i*,j}}{D_j} \right)^2 \right]. \tag{4.7}$$

With this newly constructed cost function further optimization runs were conducted in the aforementioned manner. The vector $\hat{\theta}$, subsequently referred to as our "Best Fit Parameter Set", is the parameter vector identified through iterative optimizations that minimizing our costs (see equations 4.4 and 4.3) while capturing significant qualitative behavior. The best fit parameter set is presented in detail in Appendix A.1 Tables 1 through 4.

4.4 Sensitivity Analysis and Confidence Intervals

Constructing a mechanistic model that most accurately represents the actual physical system necessitates an analysis of each parameter's influence on the model presented in Chapter 3. As the true values of θ are unknown, we evaluate our estimated parameter set $\hat{\theta}$ to determine each parameter's influence on the overall system dynamics. Biologically the surge in LH and magnitudes of E2 and T peaks hold the most significance in predicting ovulation and overall health. We use these three markers to assess the impact of perturbations to our parameters and designate the vector of their values as ω. Implementation of this approach requires the assumption of local linearity to utilize the derivatives and therefore Jacobian matrix in our calculations. We make this assumption at this time based on the apparent smoothness of the numerical approximations to our solution with the intent to revisit this assumption at such time as any unforeseen singularities are identified in our investigations.

To avoid errors in derivation of the Jacobian matrix, especially in the presence of multiple delays, we choose the finite-difference method to calculate the partial derivatives of model outputs with respect to parameters. To remain consistent, each perturbation (ϵ_n) is calculated as a percentage of the optimized parameter value previously identified. The local approximation to the derivative is then scaled by the quotient

$$\frac{\hat{\theta}_n}{\Psi(\omega, \hat{\theta})} \tag{4.8}$$

to obtain the relative sensitivities for use in rankings. The resulting equation for our sensitivity coefficients becomes:

$$S(\omega, \hat{\theta}) = \frac{\hat{\theta}}{\epsilon} \cdot \left(\frac{\Psi(\omega, \hat{\theta} - \epsilon) - \Psi(\omega, \hat{\theta})}{\Psi(\omega, \hat{\theta})} \right). \tag{4.9}$$

This method becomes advantageous when verifying results and investigating system behavior.

To get a full sense of the accuracy of our estimates, we must invoke a method that allows us to calculate a full sensitivity matrix that quantifies the relative change in our system to perturbations in our parameters. For this task we first investigate the application of inverse statistical methodology and sensitivity theory as formally presented in Frank 1978 [26] and Eslami 1994 [22] and summarized by Banks *et al.* 2007 [9].

To begin, one must calculate the Jacobian for the system in question such that each entry is of the form:

$$J_M(\theta; t)_{j,n} = \frac{\partial \Psi(t)_j}{\partial \theta_n}, \tag{4.10}$$

which denotes the partial derivative of each state variable with respect to the parameters. For delay differential equations, this construction becomes problematic and highly susceptible to errors. We can utilize the results from our original sensitivity analysis that show our delay parameters, d_P, d_{IHA}, and d_{IHB}, have been found to be approximately 1 with sensitivity coefficients $\ll 1$. An analysis of the system behavior when these delays are removed (covered more extensively in Chapter 6), reveal that the non-delay system maintains similar dynamics with only a slight reduction in period length. The analytical Jacobian after removal of the 3 delay parameters is calculated as in equation 4.10 and further denoted as $\hat{J_M}$.

Evaluated at $\hat{\theta}$, we get a $(j \times n \times i)$ matrix from which a $(j \times n)$ matrix is derived by

taking the 2-norm across our time dimension (i). We refer to the evaluated Jacobian as $S_M(\Psi(\hat{\theta});\hat{\theta})_{j,n}$, which is, by definition, our full sensitivity matrix.

We now need an estimate of the variation in our system with regards to the clinical data which is provided by Eslami 1994 [22] in the closed form:

$$\sigma_0^2(\hat{\theta}) = \frac{1}{n - n_p} \sum_{j=1}^{7} \sum_{i=1}^{28} |\Psi(t(i,j);\hat{\theta}) - y(i,j)|^2. \tag{4.11}$$

Our theory states that a covariance matrix can be constructed from the values of $\sigma_0^2(\hat{\theta})$ and $S_M(\Psi(\hat{\theta});\hat{\theta})_{j,n}$, from which the variance and standard error for each of our parameters can be extracted from the diagonal entries. The covariance matrix is of the form:

$$cov[\theta(y)] \approx \Sigma_\theta = \sigma^2[S_M^T(\hat{\theta})S_M(\hat{\theta})]^{-1}, \tag{4.12}$$

with one standard deviation for our parameter estimates as:

$$\hat{\theta} \pm SD_i(\hat{\theta}) = \sqrt{\Sigma_{ii}(\hat{\theta})}, \tag{4.13}$$

given the assumptions detailed above (continuity and error IID).

One may quickly see the challenge of our current situation in implementing this approach. A closer examination of our sensitivity matrix $S_M(\Psi(\hat{\theta});\hat{\theta})_{j,n}$, indicates that since $j < n$ then

$$det[S_M^T(\hat{\theta})S_M(\hat{\theta})] = 0$$

and $[S_M^T(\hat{\theta})S_M(\hat{\theta})]^{-1}$ does not exist. In fact, matrix theory tells us that for any given matrices A and B, $rank(AB) \leq \min\,[rank(A), rank(B)]$. Therefore the maximum number

of parameters (N) that can be analyzed through this method is bounded by

$$N \leq rank(S_M(\Psi(\hat{\theta}); \hat{\theta})_{j,n}) \leq j.$$

Overdetermined systems of this type are common in biological applications. The attempt to capture the complexity of human physiology, in particular, can lead to the development of dynamical systems with much greater dimensions than the one presented in this study. While subset selection can lead to reasonable parameter ranges, the information is incomplete at best.

We can however get a good estimate for the confidence in our parameter estimates by returning to a statistical method briefly reviewed in section 4.3, "Bootstrapping". When used for parameter estimation, a random sample, with replacement, of data is used with an original parameter set $\hat{\theta_0}$ in an ordinary least squares setting to generate a second set of estimates $\hat{\theta_1}$. The residual for each parameter set is then calculated. For the next iteration, $\hat{\theta_0}$ is chosen to be the parameter set that minimizes the residual, and the process is repeated until subsequent iterations do not improve on the model's predictions [19]. Should one anticipate a conflict in dimensionality, the series of $\hat{\theta_k}$ can provide confidence intervals for the parameter estimates. This method has been shown to converge, at a rate proportional to k [19], to the analytical values arrived at through the evaluation of Σ_θ without the challenges found in over parameterized systems. The downfall of this method is that is can be computationally burdensome and time consuming, as many reports suggest $k >> 500$ to achieve optimal results. For our purposes, we generate a reasonable sample size, with $k = 50$, as the increase in accuracy relative to the time per iteration begins to diminish for $k > 50$. Standard deviations for each parameter estimate $\hat{\theta}_n$ were then derived via MATLAB *std* function [46] and reported in full aside the values

for $\hat{\theta}$ in tables 1 through 4 in Appendix A.1.

Chapter 5

Results

5.1 Numerical Simulations: Normally Cycling Women

Given the parameters detailed in Appendix A.1 Tables 1 through 4, Figures (5.1)-(5.2) represent 60-day serum concentrations of LH, FSH, E2, P4, InhA, and InhB as predicted by the model, with daily data for mean serum levels from Welt *et al.* for comparison. Two complete 29 day cycles are presented for each hormone to support the stability conclusion.

Predicted serum T concentrations for a 30 day simulation follow in Figure 5.3. Approximated T levels increase from a day 3 level of 30 $^{ng}/_{dL}$ to a maximum level of 44 $^{ng}/_{dL}$ on day 11 of the cycle. After ovulation, T slowly declines, plateauing from day 17 to 22 at approximately 34 $^{ng}/_{dL}$. At the end of the luteal phase, levels continue to decline before a slight rebound in circulating levels is observed during the luteal to follicular transition. Figure 5.3 presents data extracted from Sinha-Hikim *et al.* [73] against model predictions

for comparison.

One can ready observe the qualitative similarities to clinical observations for all seven hormones. The solution presented remains oscillatory and stable. At this time, the solution presented is the only stable periodic solution identified for the Best Fit Parameter set $\hat{\theta}$. This is contrary to the findings of Harris-Clark [33], who identified 2 stable periodic solutions for the original merged delay system. In subsequent expansions of the Harris-Clark model, Pasteur [58] and Margolskee [45] report a single stable periodic solution. While we do not discount the existence of a second solution at this time, we do acknowledge the very narrow basin of attraction identified for the second Harris-Clark solution and the possibility that if the solution persists given the current expansion, it has at this time, eluded our detection.

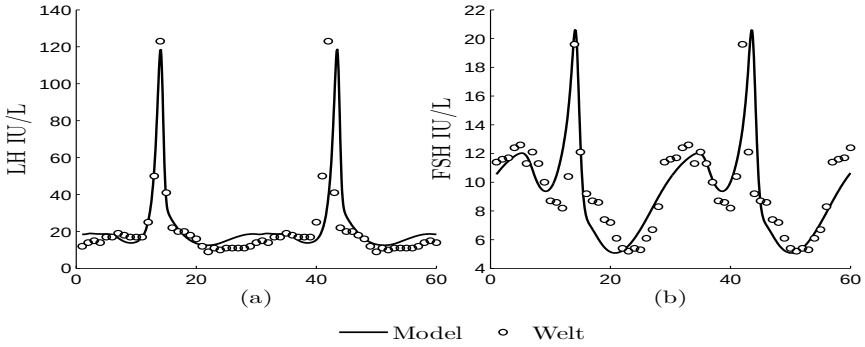

Figure 5.1: Two 29-day cycles for (a) LH data from Welt *et al.* (∘)and (b) FSH data from Welt *et al.* (∘) are presented with current model simulation (solid curve).

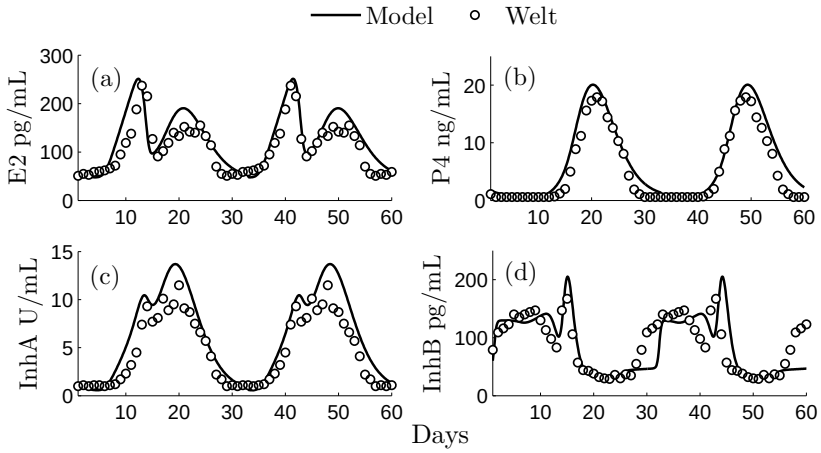

Figure 5.2: Two 29-day cycles for (a) E2 data from Welt *et al.* (∘) , (b) P4 data from Welt *et al.* (∘) , (c) InhA data from Welt *et al.* (∘), (d) InhB data from Welt *et al.* (∘) are presented with model simulations (solid curve).

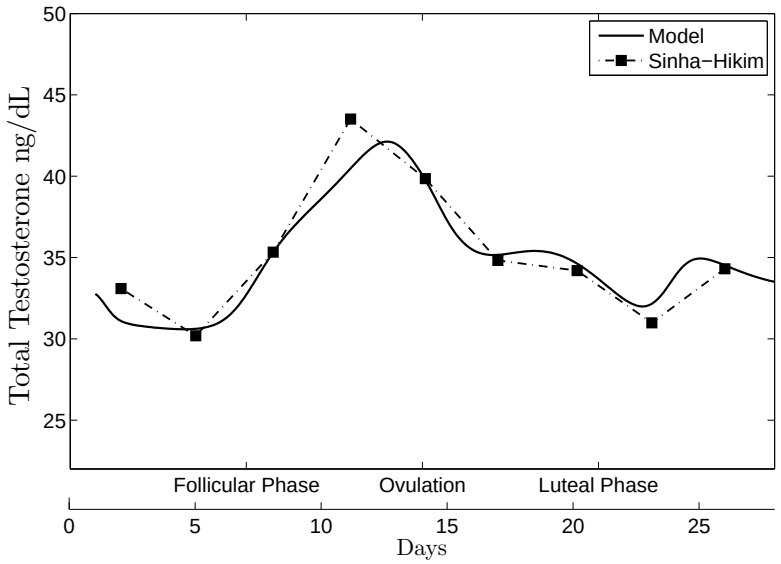

Figure 5.3: T data from Sinha-Hikim *et al.* (■) 9 data points, (– · –) linear interpolation with current model simulation (solid curve)

5.2 Modeling Predictions: Stockpiling of Follicles

Irregularities in cycle length are commonly seen in patients with PCOS. As a common cause of infertility, PCOS affects up to 10% of reproductive age women and significantly correlates with increased risk of Type II diabetes and its associated morbidity [1, 5, 57]. Common phenotypes of PCOS also include elevated androgens and the appearance of polycystic ovaries on ultrasound [4], both significant components in the etiology of PCOS [34, 48, 65]. Histological studies of tissue samples taken from clinically diagnosed PCOS patients, recently reported by Maciel *et al.* [44] suggests a "stockpiling" of preantral follicles when compared to controls. Their findings show a significantly, ($P = .001$), increased number of follicles comprised of an oocyte and a single layer of cuboidal granulosa cells, typically classified as primary follicles. It is hypothesized that the increase in primary follicle numbers is due to slower growth during this stage, represented by PrA1 in our model. We investigate m_2 as a possible model parameter to test this hypothesis. As a measurement of mass transfered out of the primary stage, decreasing m_2 should delay primary follicle maturation, permitting additional growth of primary follicles.

For comparison, we begin by presenting LH concentrations from the stable periodic solution that best fits data from Welt *et al.* and Sinha-Hikim *et al.* in Figure 5.4. Using the parameters listed in Appendix A.1 Tables 1 through 4, our best fit solution over 7 months has an average cycle length of approximately 29 days. This is consistent with reports from Baerwald *et al.* and Gougeon *et al.* that report an average cycle length of 27-32 days [6, 31]. We assume ovulation coincides with the LH surge given a follicle of sufficient size is available for rupture. As the exact surge level of LH necessary to induce ovulation is unique to each woman, we identify (by thick horizontal lines) LH levels

at 75% and 50% of the mean maximum LH level reported by Welt *et al.* for possible threshold references. While the ovarian mass values for PrA1 through SmAn (Figure 5.4) are unitless we note that the first preantral follicle mass peaks at approximately 20 units before transferring to the second androgen dependent preantral follicle mass. Follicular mass during this time is presented to demonstrate the interaction between the mass of developing follicle and ovulation assuming that surge levels of LH are indicative of the existence and timing of ovulation.

Figure 5.5 demonstrates the effect of reducing m_2 by approximately 50% of the best fit value in Table 3. Analysis of the resulting behavior, over 8 months, reveals an LH surge exceeding 150 $^{\text{IU}}/_{\text{L}}$ followed by a surge approximately 20 $^{\text{IU}}/_{\text{L}}$ lower. While each peak surge occurs monthly, the pattern of alternating surge levels takes over two months to repeat. Similarly the first preantral follicle mass begins to oscillate with a maximum mass of 30 units that results in lower mass transfer to the second preantral mass. In the normal case, our cycle length and the time for LH levels to return to the peak level of the previous cycle were the same. Reducing the transfer rate from PrA1 approximately doubles the time between peaks of the same magnitude, a phenomenon known as a period doubling event (the period of the solution to our model equations is now $\sim$ 64 days). Identification of this behavior is mathematically significant for systems of this size and complexity. Although period doubling often occurs in systems of non-linear equations, it has rarely been demonstrated in a physiological model which predicts data in literature. Demonstrated in Figure 5.6, reducing m_2 to 30% of the best fit value in Table 3, results in LH surges of four distinct values. In this simulation the pattern of peak variation now repeats every 5.5 months with an average time between surges of approximately 40 days (another period doubling has occurred). Examination of the resulting follicular mass reveals a distinct pattern of elevated PrA1, stockpiling or preantral follicles, that

completes its transfer to subsequent stages over a period of approximately 80 days suggesting correlation between preantral growth and irregular menstrual cycles consistent with the hypothesis of Maciel *et al.* [44]. Mathematically this behavior highly suggests the existence of a period doubling cascade, or a doubling in the duration necessary for LH to return to its initial value.

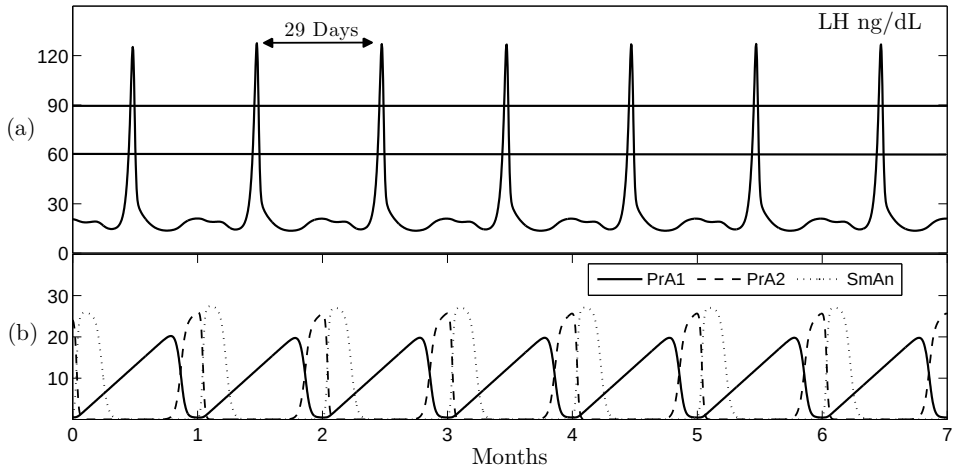

Figure 5.4: (a) Simulated serum LH IU/L over 8 months with reference lines for 75% and 50% of mean Welt surge levels (b) First 3 stages of follicular development (PrA1, PrA2, and SmAn)

Complex dynamical systems with period doubling cascades are often associated with chaotic behavior [67]. Investigating this phenomenon motivated numerical experiments with additional decreases in m_2 to identify behavior consistent with chaotic attractors. Reducing of m_2 by an additional 5% causes the disappearance of the stable 4 cycle shown in Figure 5.6 and the appearance of a chaotic attractor as demonstrated in Figure 5.7.

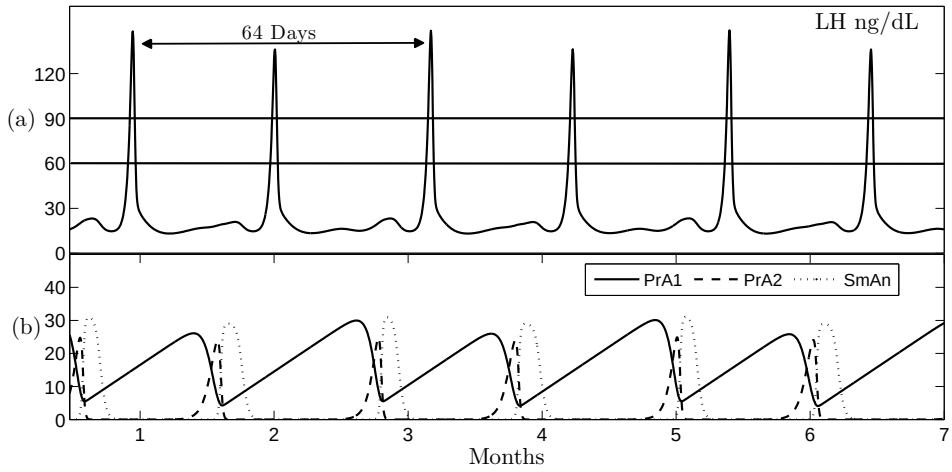

Figure 5.5: (a) Serum LH level results after a 50% reduction in parameter m_2 from best fit value in Table 3 (b) Note the increase in PrA1 from Figure 5.4

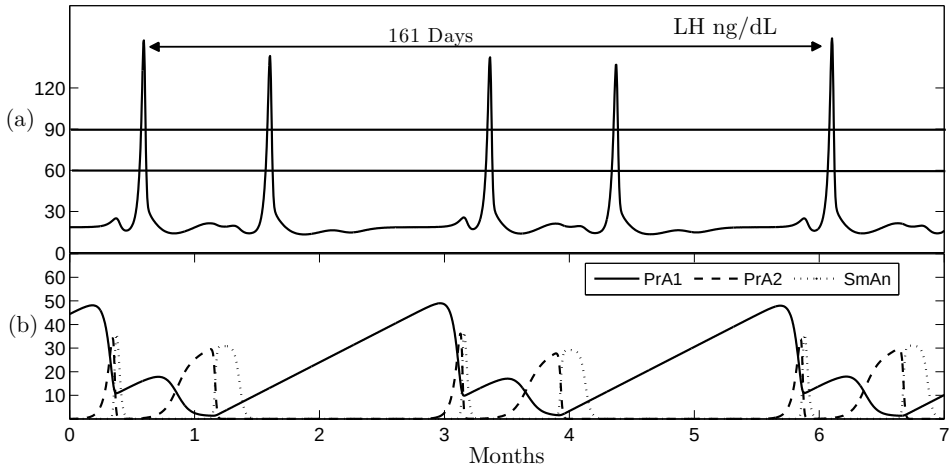

Figure 5.6: (a) Serum LH level results after a 70% reduction parameter m_2 best fit value in Table 3 (b) First three stages of follicular development.

Verification that the apparent attractor was formally chaotic was achieved by the identification of a 3 cycle that exists in a very narrow range of m_2 values near 26% of the value

reported in Table 3. (Due to the lack of biological relevance of the 3 cycle solution, the results are not presented, merely noted.) If one assumes an LH threshold at 75% of the reported mean, as demonstrated by the top horizontal line, the solution presented would ovulate approximately 5 times per year given the availability of a dominant follicle at the time of LH surge. Reducing the threshold assumption to 50% increases the frequency of ovulation to an average 8 cycles annually over the three year window presented. These frequencies are consistent with a clinical diagnosis of oligomenorrhea, infrequent menstruation with 4-8 menstrual cycles per year, a primary phenotype of PCOS. The appearance of low amplitude peaks that do not exceed threshold values observed in Figure 5.7 may be consistent with non-ovulatory LH surges discussed in Baerwald *et al.* 2012 [7].

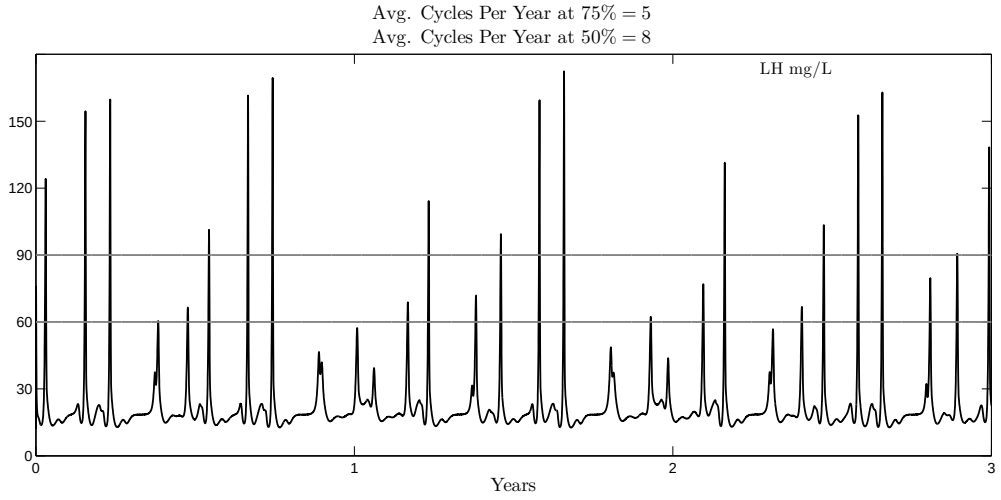

Figure 5.7: Chaotic serum LH levels observed over 3 years as m_2 is reduced to 25% of the best fit value best fit in Table 3. If ovulation occurs for an LH surge over 90 mg/L (75 % of the normal LH surge) then $\sim$ 5 ovulations occur per year. If ovulation occurs for an LH surge over 60 mg/L then $\sim$ 8 occur per year.

5.3 Model Predictions: Pharmacodynamics

In the development of any mathematical model in a biological setting, it is important, yet sometimes difficult, to validate the model's ability to reproduce real life observations. For our model, we are fortunate that much is known about the effects of combined oral contraceptives on the menstrual cycle. The necessity of an LH surge in inducing oocyte release is widely accepted [42, 82, 88] and a common pharmacological target. Suppression of this surge has historically been achieved by the administration of synthetic estrogens and progestins that disrupt the normal cyclic pattern of LH. It is advantageous to use this knowledge as a benchmark for the validity of any model of the female menstrual cycle.

5.3.1 Combination Oral Contraceptives

We have chosen to investigate the simulation of estrogen / progestin based oral contraception. To simulate an oral contraception's (OC) effect we must first consider of the pharmacodynamics of the component drugs. Many contraceptives currently on the market in the U.S. contain a combination of ethinyl estradiol (EE) and Levonorgestrel (LNG). Dosages for each compound range between $20 - 35\ \mu g$ and $0.1 - 0.15\ mg$ respectively, and are traditionally referenced as a ratio of progestin/EE. Effectiveness of the compound products may vary due to differences in absorption, distribution, metabolism, and excretion (ADME), not only for individual patients, but for each compound. Pharmacokinetic (PK) studies provide information that helps us determine the biological impact of synthetic hormones in relation to their natural cousins. Dose response curves help quantify ADME for each drug so that we may determine how much, if any can be detected in the serum and at what rate clearance occurs. In a 2010 study by Westhoff *et*

al. [85], 30 women of varied BMI were recruited for a 24 hour PK study of a monophasic 1.5/30 combination oral contraceptive. Participants completed $2-3$, 21 day cycles of treatment before a 24 hour PK study conducted within day $15-21$ of the study cycle. Results show EE serum levels range between 35 $^{pg}/_{mL}$ to 115 $^{pg}/_{mL}$ with an area under the curve (AUC) of 1413.7 $^{pg \cdot h}/_{mL}$, with LNG ranging between 2.5 $^{ng}/_{mL}$ and 7.0 $^{ng}/_{mL}$ with an AUC of 85.8 $^{ng \cdot h}/_{mL}$ [85]. Once in circulation hormones have bioactivity that can be quantified and reported as a relative binding affinity, or RBA. For the compounds we wish to simulate, we must take into consideration that LNG has a 323% RBA for the progesterone receptor and a 58% RBA for the AR when compared with progesterone and testosterone respectively [74], while EE is reported to have an RBA of 190% when compared to E2 [10]. To simulate the use of OC within the framework of our system we must take into account both the pharmacokinetics and RBA of both LNG and EE.

We begin by constructing a function that will turn on and turn off a dose of hormone. MATLAB's *heaviside*, or step function, will allow us to perturb our system in a time dependent manner that reflects the typical OC pattern of 21 days on and 7 placebo. This function acts as a switch, where the only two values are 0 or 1. We acknowledge this function does not accurately capture the dose response curve that we see in PK studies, yet given the time scale of our system and the intent to utilize the results for validation purposes only, we feel it is sufficient at this time. The magnitude of the perturbation is calculated as a function of the dose response levels and the RBA.

We know that 0.15 mg dose of LNG translates to an average serum level of 3.5 $^{ng}/_{mL}$, and a 30 mg dose of EE results in a mean serum level of 58.9 $^{pg \cdot h}/_{mL}$ [85]. We must adjusts these estimates to reflect any reduction of bioavailability. For LNG, current studies show that 100% of the compound remains unbound, while EE has a 97% bioavailability. In estimating the magnitude of the step function, we therefore set the magnitude of our step

function to 3.5 and 57 respectively.

The question now becomes at which point in our model do we introduce this function. The obvious points of entry would be at the baseline production rate of our auxiliary equations, but we know that these compounds have varying, and multiple receptor affinities that must be considered. To account for these variations, we scale each of the above magnitudes by the reported RBA for each the the respective sex steroid receptors and create an additional step equation to reflect androgenic activity of LNG. We now have three magnitude coefficients:

- $m_{EE} = 57 \cdot 1.90 = 108.3$
- $m_{Lp} = 3.5 \cdot 3.23 = 11.375$
- $m_{Lt} = 3.5 \cdot 0.58 = 2.03$

that are used to simulate the systemic affects of LNG and EE at auxiliary coefficients e_0, p_0 and t_0 respectively. We begin the simulation at day 7 of the third cycle to insure the system is on the stable periodic orbit. In Figures 5.8 and 5.9 we demonstrate the behavior of the system before and after administration of the simulated OC. In Figure 5.8 we present serum levels of LH (a.), E2 (b.) and T (c.) as predicted by the model using the best fit parameter set $\hat{\theta}$ over an eight month period. Additionally, we present the model predictions of ovarian mass for the dominant follicle (DmF), ovulation (OvF), and the second stage of CL, development ($CL2$) in panel (d.).

In Figure 5.9, we present model predictions of the above hormones and ovarian stages during a three month period of OC administration simulated by the dose curve in panel (e.) of figure 5.9.

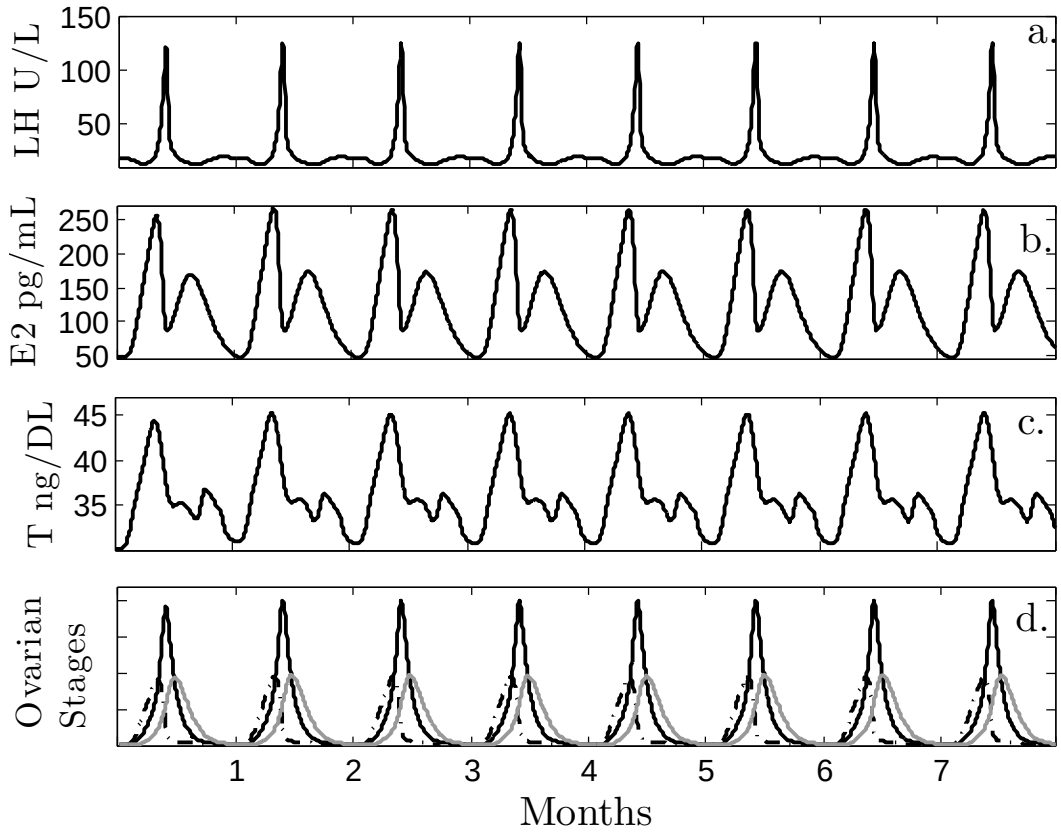

Figure 5.8: Serum level predictions for (a.) LH , (b.) E2 , and (c.) T are presented over an 8 month period for the best fit parameter set. (d.) Follicular mass predictions for ovarian growth stages DmF, OvF, and $CL2$ are shown to demonstrate the rapid increase in follicular growth that coincides with ovulation.

In Figure 5.9 we notice what appears to be surges in LH at the first day of OC administration. Should this be due to a "shock" to the system, it occurs on day seven of the cycle, as panel (d.) suggests, there is not a viable dominant follicle for rupture. This may though, simply be an abnormality in the numerical algorithm underlying the

delay differential equation solver we are utilizing in response to the shape of the *heaviside* function. Regardless of this abnormality if one looks at panel (a.) from both figures, it is apparent serum LH experiences a major reduction in surge levels during the time of OC administration, and begins to return to normal cyclicity upon the removal of the stimulus. The profile for E2 in both panels (b.), shows decreasing levels of E2 in the system during OC use, as in T as represented in panel (c.) of both figures. We also note the return of both to their normal levels once the OC is removed from the system. In the (d.) panels it of interest to note that the mass of the dominant follicle before and during ovulation has significantly diminished, possibly reflecting the absence of a viable follicle for ovulation.

As a validation tool, the above simulation increases our confidence in the model presented in chapter 3. We can see that under well documented circumstances the model predicts the suppression of the LH surge and follicular development during OC use. Moreover, model predictions of a return the regular cyclicity in approximately 3 months after termination of treatment is within the range reported by Gnoth *et al.* and Wiegratz *et al.* that observed a return to normal cyclic function, determined by cycle length or successful pregnancy respectively, occurring between 1 to 9 months [30, 86].

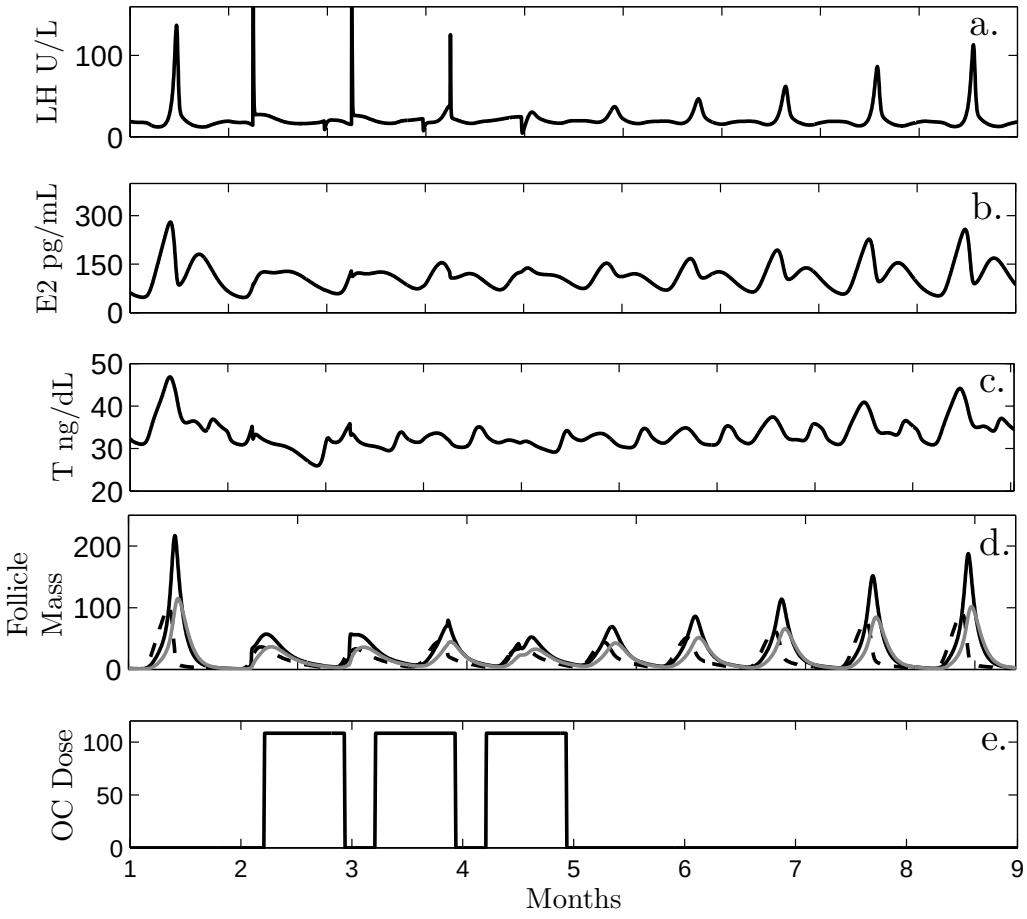

Figure 5.9: Serum level predictions for (a.) LH , (b.) E2, and (c.) T are presented over an 8 month period for the best fit parameter set with the introduction of a simulated three month monophasic dose of a combination $\cdot^{15}/_{30}$ OC. (d.) Follicular mass predictions for ovarian growth stages DmF, OvF, and $CL2$ are shown demonstrating the reduction in follicular growth during OC administration. (e.) Graphic representation of EE serum levels as introduced into the model. LNG introduction not graphically represented.

Chapter 6

Bifurcation Analysis

Here we investigate in more depth the dynamical behavior of this new model. We study the stability and instability of periodic solutions, bifurcations resulting from variations in sensitive parameters, and the existence and significance of hysteresis curves in bifurcation diagrams.

Normalized sensitivity coefficients for the system (eqs. 3.1 - 3.12), computed in Chapter 4, estimate the amounts of variation in system outputs with respect to small variations in system parameters. In a mathematical sense, a normalized sensitivity coefficient is a partial derivative of the state variable equations with respect to the parameters, normalized so that comparisons may be made. The only nonzero time-delay parameters were of duration 1 day for the inhibitions of P4, InhA, and InhB in eqs. 3.13 and 3.16. The normalized sensitivity coefficients for these delay parameters, d_P, d_{InhA} and d_{InhA}, were at most 0.1 and quite small when compared with sensitivities of 1 or larger (see Appendix A.3 Table 7). Thus, for this study, we set the time-delays equal to zero and refit system parameters to the data of Welt *et al.* [84] and of Sinha-Hikim *et al.* [73] to obtain the values in Tables 10 through 13 in Appendix A.5, further referred to as $\tilde{\theta}$. Figure 6.1

compares the solutions for both parameter sets, $\hat{\theta}$ and $\tilde{\theta}$ against our clinical data. One can see that removal of the delays shortens the period of the stable solution, but does little to affect the overall behavior of the system or qualitative agreement with the data. Henceforth, we study equations (3.1-3.12) with the parameter set $\tilde{\theta}$ and zero time-delays.

LH and E2 simulations for this model exhibit two locally asymptotically stable periodic solutions (Figure 6.2). One solution (the dashed curves in Figure 6.2) approximates well the data of Welt *et al.* [84], has a period of 27 days, and represents a menstrual cycle for which ovulation occurs. The other periodic solution (the solid curves in Figure 6.2) has a period of approximately 23 days and represents an anovulatory cycle due to the lack of LH surge. We refer to these solutions as the normal and the abnormal cycle, respectively. Notice that E2 levels for the abnormal cycle vary slightly over the month and remain below 150 ng/dL. On the other hand, the follicular E2 of the normal cycle exceeds 230 ng/dL a level which elicits an LH surge. For the abnormal cycle FSH and P4 concentrations are lower than those of the normal cycle (results not shown). These characteristics are present in many PCOS individuals (see Yen (1999) and Marshall *et al.* (2001)). Bistability of this type has been observed for similar hormone control models by Harris-Clark *et al.* [33] and Selgrade *et al.* [70]. As illustrated in [33], the abnormal cycle may be perturbed to the normal cycle by the administration of exogenous P4 during the luteal phase and the normal cycle may be perturbed to the abnormal by exogenous E2. Moreover, small variations in sensitive parameters may result in bifurcations which remove the abnormal cycle, producing a model with a unique asymptotically stable solution that represents an ovulatory menstrual cycle. Motivated by the findings of Harris-Clark *et al.* [33], and the identification of two stable periodic solutions for our zero time-delay parameter set $\tilde{\theta}$, we seek to identify similar behavior that may lead to increased un-

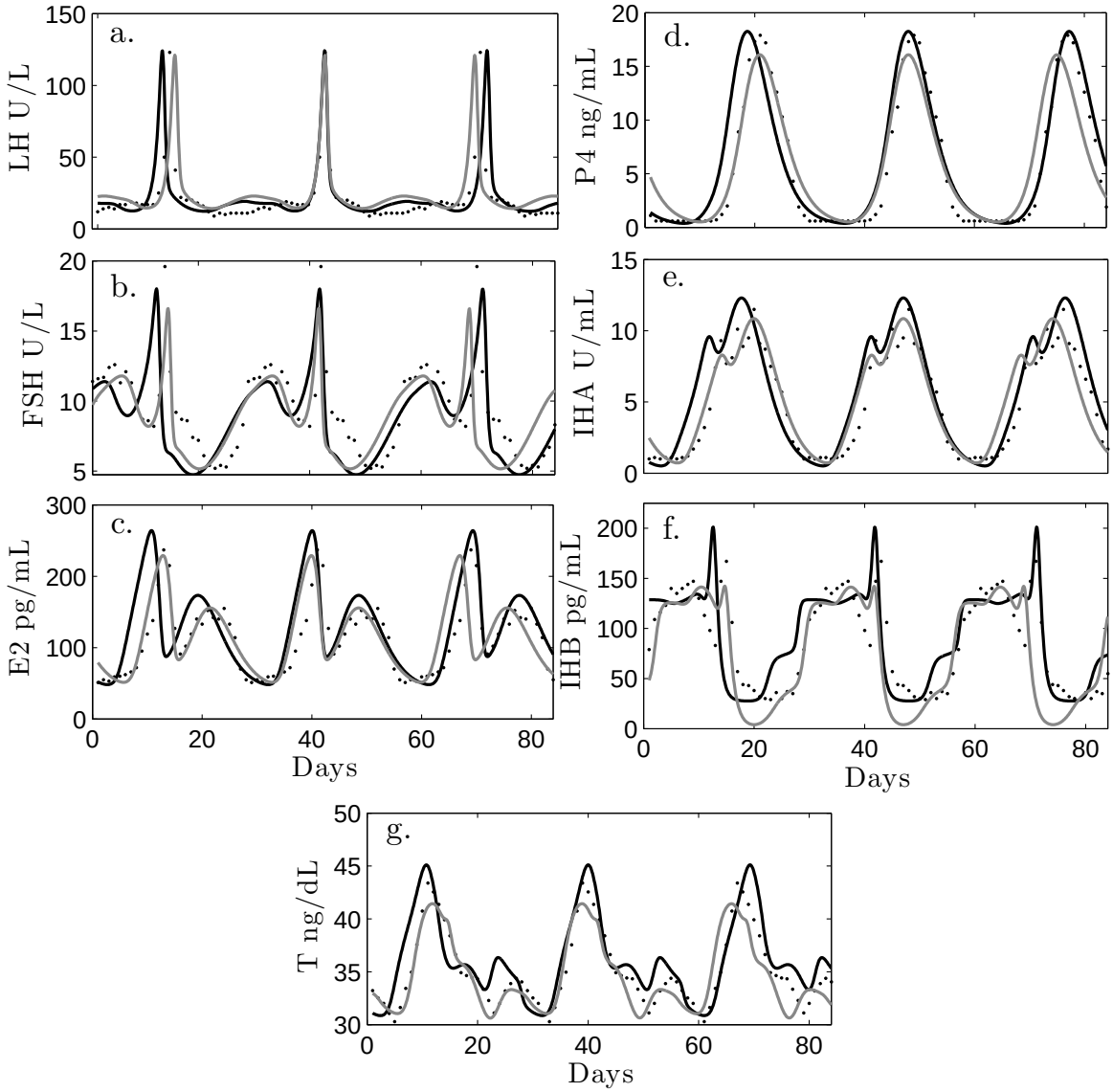

Figure 6.1: For comparison purposes, model predictions are presented with (black lines) and without delays (grey lines) against clinical data (·) from Welt *et al.* and Sinha-Hikim *et al.*.

derstanding of conditions similar to PCOS. In this chapter we look at the parameters identified as "highly" sensitive and explore the biological significance of the associated

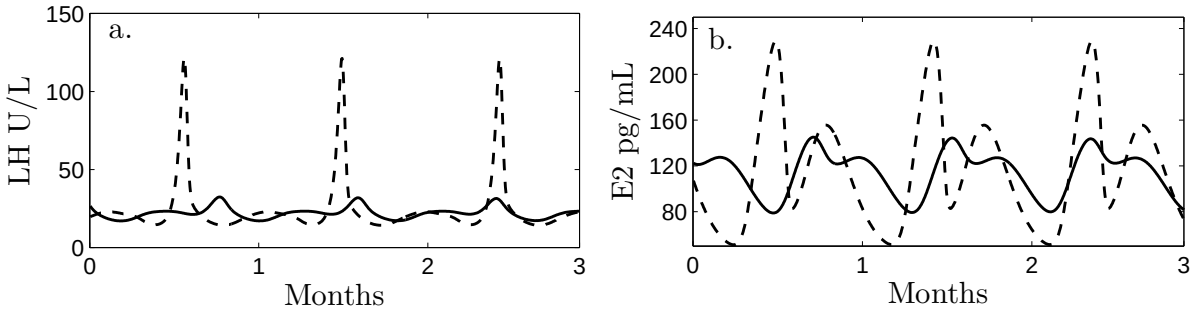

Figure 6.2: E2 and LH model simulations for (eqs. 3.1-3.12) with zero time-delays for 3 months. The dashed curves depict normal cycles and the solid curves, abnormal cycles.

bifurcations. Many of the parameters identified in our analysis were thoroughly analyzed by Harris-Clark *et al.* [33], therefore we choose to focus on the parameters associated with the current model expansion and/or PCOS. We begin with a formal study of the period-doubling bifurcation introduced in Chapter 5 for m_2, followed by an extensive investigation of multiple bifurcations associated with κ and varying follicular production rates of T.

6.1 Bifurcation Theory: A Brief Overview

The term bifurcation and its study were first introduced in 1885 by Henri Poincaré [61], as a way to study changes in topological structures. To fully understand dynamical systems and bifurcation analysis is a task for which a single life time can not begin to tackle. Poincaré himself left many unsolved problems including his most famous, the Poincaré Conjecture about 3-manifolds whose solution afforded Russian mathematician Grigori Perelman the Fields Medal in 2006, almost one hundred years after it was posed. With that in mind, a basic understanding of the terminology and theory utilized in our subse-

quent sections is well within our grasp and an appropriate discussion before we proceed. To begin let us review the definitions intrinsic to our study.

- **Dynamical System:** A mathematical formulation of a deterministic process. The set of all possible states and the law that governs their evolution through time.
- **Phase Space:** All possible states of a dynamical system. A continuous state space.
- **Equilibrium:** An element in the function's domain that is mapped to itself by the function, also referred to as a fixed point.
- **Limit Cycle:** A trajectory in the domain of the function such that the function value returns to that point after a finite number of iterations.
- **Bifurcation:** The division of something into 2 paths or branches.
- **Poincaré Map:** The intersection of a periodic orbit with a lower dimensional subspace (return map).

We defined our dynamical system in Chapter 3. We have identified a single periodic solution, or limit cycle, that satisfies the conditions determined by our system (see Figure 6.2). Now we would like further understanding of the phase space in which our solutions reside. To begin, we first calculate the Jacobian (J) of the system. This allows us to apply well established methods from linear algebra, for an efficient exploration of our phase space. Unlike in Chapter 4 where the entries used are the partial derivatives of our system equations in respect to the parameters $\hat{J_M}$, for the current analysis, we construct the entries of the current Jacobian as the partial derivatives of our system equations in respect to each of the state variables, and denote it as $\tilde{J_M}$. This approach provides a

linear approximation for the gradient in a small neighborhood of each element in our phase space. Once calculated, we evaluate $\tilde{J_M}$ at a point of interest in our phase space. The eigenvalues (λ_j) of the evaluated $\tilde{J_M}$ reveal the direction of the gradient around that point.

Equilibria are classified based on the values of λ_j for their respective evaluated $\tilde{J_M}$. Many types of equlibria have been well studied in three dimensional space, and are often analogous to higher dimensions. For our purposes, we will not review them in their entirety, but briefly mention two of immediate relevance; saddles and nodes. For nodes, all the corresponding λ_j will be either positive or negative, denoting an unstable or stable fixed point respectively. Saddle nodes are much more interesting. For a saddle node to occur in a system, it first must be of dimension $j \geq 2$, and secondly, it must have a set of three λ_j such that there is a single zero value, a positive value, and a negative value. The eigenvector associated with $+\lambda$ determines the direction solutions travel from the point, whereas the eigenvector associated with $-\lambda$ gives us the direction from which solutions travel to it.

We are interested in bifurcations of the system for three main reasons:

- Bifurcations are points where small changes in a parameter can result in large changes in our system dynamics.
- The bifurcation parameter and value provide important information about how trajectories change or can be changed to direct a system in a new direction.
- Pure mathematical curiosity and wonder.

We track these occurrences by monitoring the behavior of the eigenvalues. Should a complex conjugate pair of eigenvalues exists associated with an equilibria, their path

through the imaginary axis suggest the existence of a Hopf bifurcation [40, 78]. Hopf bifurcations often signal the transition from non-oscillatory solution to a periodic limit cycle. The limits cycles themselves may undergo bifurcations, saddles node bifurcations, torus bifurcations and period doubling bifurcations to name a few.

The analysis of higher dimensional bifurcations, in phase spaces of many dimensions, with a significant number of parameters can efficiently be conducted using numerical packages. Previously, most of our work has been conducted using numerical solver packages available through MATLAB [46]. For this purpose, we have found it more efficient and user friendly to switch our tool of choice to the AUTO package available through XPP [21]. In tracking bifurcations with respect to a candidate parameter, XPPAUT approximates a solution to the given system and analyzes the eigenvalues of the linearized Jacobian near that solution to determine the direction to perturb the parameter in search for changes in the eigenvalues, or bifurcations. It designates the type of solution found graphically as a function of a chosen output (y-axis) and the parameter (x-axis). In the output graph equlibrium solutions are represented with single dots ($\cdot$), while limit cycles are circles ($\circ$) on the graph. For all of the following investigations, the height of the LH peak is chosen as an easily identifiable and biologically significant output to monitor.

6.2 Bifurcation Analysis for Parameter m_2

In Chapter 5 we showed how varying the sensitive parameter m_2 produced significant changes in model behavior. Decreasing m_2 delays the growth of preantral follicles and results in a "stockpiling" of these small follicles as observed by Maciel *et al.* [44] in PCOS women. Figures 5.4 through 5.7 illustrate a period-doubling cascade of bifurcations resulting in apparent chaotic menstrual cycle behavior. Here we examine the bifurcation

diagram with respect to m_2 using the software XPPAUT [21], which is appropriate for systems without time-delays. The XPPAUT solver uses an adaptive Newton method with a default tolerance of $1e-3$ which approximately equals the best-fit value $m_2 = 0.000868$. To avoid scaling conflicts, we investigate the *log* transform for this parameter $l_2 = \log(m_2)$ where log is the natural logarithm function. This transformation brings the scale of our bifurcation parameter to $-1e+1$, well away from the tolerance of our integrative solver. Our bifurcation diagram (Figure 6.3) plots maximum LH along a periodic or equilibrium solution against l_2.

We address the findings of our bifurcation diagram from max to min on the x-axis to agree with the perturbation direction for l_2. For values of l_2 larger than -5.66, the only stable solution is an equilibrium (the solid line in the lower right of Figure 6.3), which represents an anovulatory cycle due to the insufficient LH surge. A saddle-node bifurcation (upper SN) of periodic solutions occurs at $l_2 = -5.66$ resulting in a line of stable limit cycles (upper curve) and unstable cycles (lower curve) as l_2 decreases. The stable cycles are ovulatory and continue through the value of $l_2 = -7.05$ that corresponds to the normal cycle (large $\Diamond$ in Figure 6.3) presented in Figure 6.2. At $l_2 = -6.81$, the stable equilibrium undergoes a Hopf bifurcation (HB) which results in a stable periodic solution (solid curve) and an unstable equilibrium (the lighter line that continues to the left from HB). This stable anovulatory cycle exists until $l_2 = -7.17$ where it coalesces with the unstable cycle and both disappear via a saddle-node (lower SN). For l_2 between -7.54 and -7.17, the only stable solution is the ovulatory cycle along the upper portion of the figure. At $l_2 = -7.54$, a period-doubling bifurcation (PD) causes the stable ovulatory cycle to destabilize and a stable solution of twice the period to appear (curve branching off below first PD). It is believed to correspond to a 2-cycle solution similar to the one identified in the delay model (see Figure 5.5). More period-doublings occur as l_2 decreases

through -7.72 and through -7.74. The period-doubling cascade and implications are discussed in full in Chapter 5, Section 5.2.

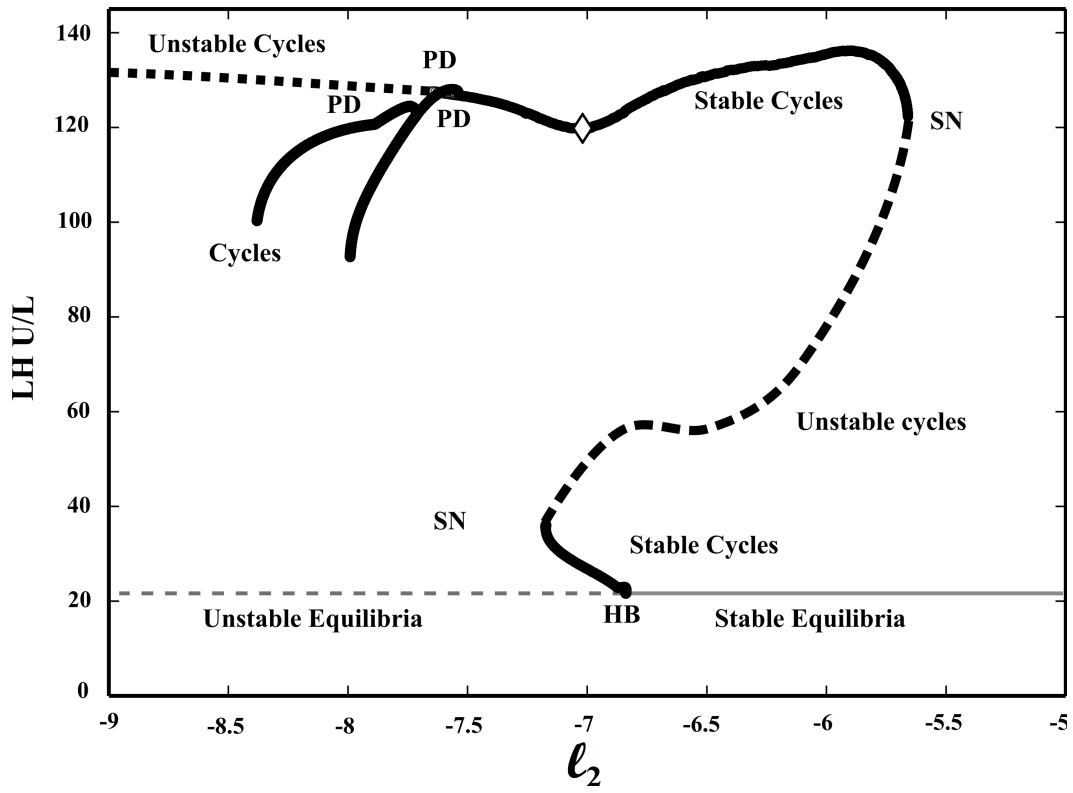

Figure 6.3: Bifurcation diagram with respect to $l_2 = \log(m_2)$ for eqs. 3.1-3.12 with remaining parameters from zero time-delay set $\tilde{\theta}$. HB, SN an PD denote Hopf, saddle-node and period-doubling bifurcations. The large $\Diamond$ indicates the position of the normal cycle for the parameter set $\tilde{\theta}$.

The sigmoid shaped curve in the right half of Figure 6.3, which contains stable and unstable cycles, is referred to as a hysteresis curve or loop. For each l_2 value within the

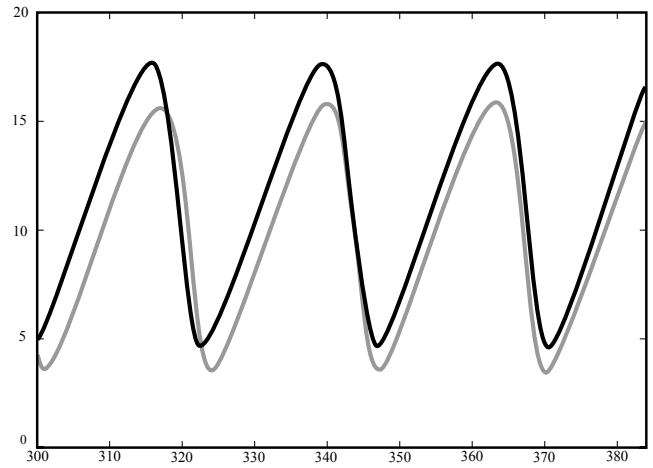

Figure 6.4: The first preantral follicular stage $PrA1$ is plotted for $l_2 = -7.13$ (grey curve) and for $l_2 = -7.3$ (black curve). A slight increase in preantral follicular mass occurs as l_2 decreases.

branch of the hysteresis curve between SN ($l_2 = -7.17$) and HB ($l_2 = -6.81$), there is a stable normal cycle (large amplitude LH) and a stable anovulatory cycle (small amplitude LH). A woman whose cycle is represented by one of these stable anovulatory cycles may be perturbed to a normal cycle by decreasing her l_2 parameter below -7.17, which effectively increases the stockpiling of her preantral follicles. However, additional stockpiling where l_2 becomes less than -7.54 results in irregular or chaotic cycling because of the period-doubling cascade. Figure 6.4 plots the first preantral follicular stage for $l_2 = -7.13$ (dashed curve) and $l_2 = -7.3$ (black curve) showing a slight increase in follicular mass as l_2 decreases. This observation suggests a curious biological hypothesis that a woman, who is anovulatory with insufficient LH, may benefit from additional preantral follicular mass but only up to a point after which too much mass may lead to irregular cycling. This suggestion is indicative of the delicate balance necessary to maintain normal reproductive function.

6.3 Bifurcation Analysis for Parameter κ

The parameter κ in eq. 3.13 modulates the affect of T on baseline LH synthesis via the term T^{κ}. Since the best-fit parameter value $\kappa = 0.9176$ is positive but less than one, this synthesis rate increases with T and with κ but is slightly sublinear. Values of $\kappa > 1$ magnify this affect and reduce the inhibitory effect of P4 on LH synthesis, as it appears in the denominator of our equation RP_{LH} (see eq. 3.13). Here we examine the bifurcation diagram (Figure 6.5) which plots maximum LH along a periodic or equilibrium solution against κ. As in the previous section we conduct our study along the direction of the parameter perturbation, this case along the x-axis from min to max.

For values of κ less than 0.883, the only stable solution is an equilibrium (the solid curve labeled 'st. eq.' in the lower left of Figure 6.5), which represents an anovulatory cycle since LH peaks below levels necessary for ovulation. At $\kappa = 0.883$, a Hopf bifurcation (HB) occurs which results in a stable periodic solution (solid curve) and an unstable equilibrium (the lighter curve that continues to the right from HB). This anovulatory stable cycle exists until $\kappa = 0.924$ where it coalesces with an unstable cycle and both disappear via a saddle-node (lower SN). The unstable cycle originates from a saddle-node (upper SN) at $\kappa = 0.899$, which also produces the stable ovulatory cycle that continues to the normal cycle (large $\Diamond$). The system maintains the stable ovulatory cycle as κ increases to 1.065, where a torus bifurcation (TR) occurs. This bifurcation is a Naimark-Sacker bifurcation [50, 66] of the return map of the periodic solution which destabilizes the periodic solution and surrounds it with an attracting invariant torus. Solutions on the torus approximate the periodic solution but, generally, may be periodic or irregular. Between the two TR's, i.e., for $1.065 < \kappa < 1.197$, the only attractor for the system in eqs. 3.1 - 3.12 is the invariant torus. For parameters just to the left of the left TR, the

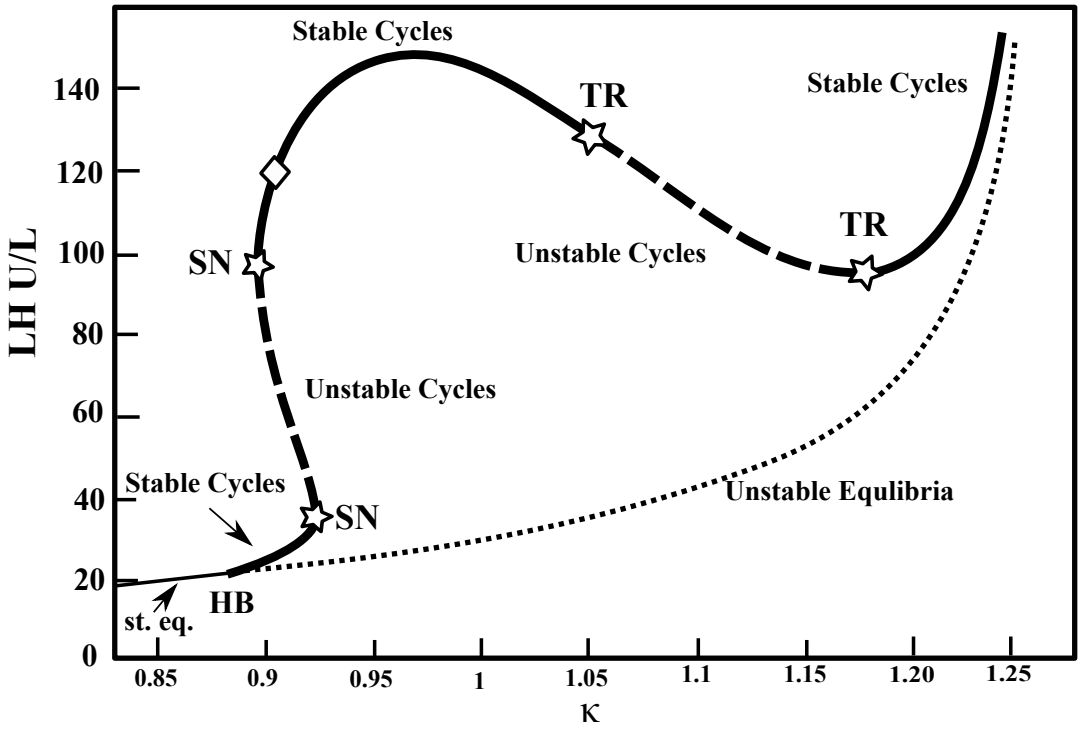

Figure 6.5: Bifurcation diagram with respect to κ for eqs. 3.1 - 3.12 with remaining parameters from $\tilde{\theta}$. HB, SN an TR denote Hopf, saddle-node and torus bifurcations ($\star$). The large $\Diamond$ indicates the position of the cycle for the parameters of Appendix A.5 Tables 10 through 13.

stable ovulatory cycle (see Figure 6.6 for $\kappa = 1.05$) has a period of about 27 days and is similar to the stable cycle (Figure 6.2) for the parameter set $\tilde{\theta}$. For parameters just to the right of the left TR, the stable periodic solution on the torus (Figure 6.6) at $\kappa = 1.1$ has a period of approximately 78 days and represents three ovulatory menstrual cycles of differing LH surge heights. When $\kappa = 1.15$, the stable solution on the torus (Figure 6.7) is not periodic but LH reaches at least 75% of normal surge height every 23 to 27 days.

Such irregular cycles may still be ovulatory and may be a more realistic representation of a woman's menstrual cycles. At $\kappa = 1.197$ the TR is a reverse torus bifurcation where the attracting torus shrinks to a periodic solution. This stable cycle, which is plotted in Figure 6.8 for $\kappa = 1.21$, has a period of about 20 days and LH levels ranging between 50 IU/L and 92 IU/L.

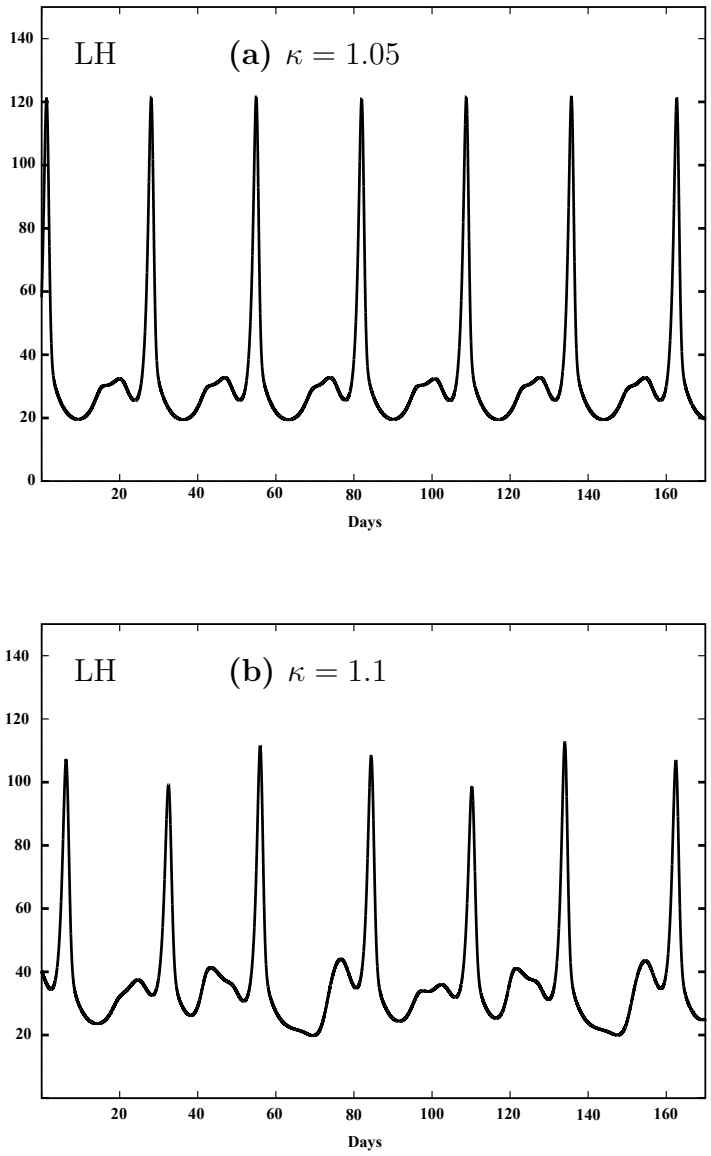

Figure 6.6: LH model simulations for eqs. 3.1 - 3.12 with zero time-delays. (a) $\kappa = 1.05$ and cycle has a period of about 27 days. (b) $\kappa = 1.1$ and the solution has a period of about 78 days which represents 3 menstrual cycles.

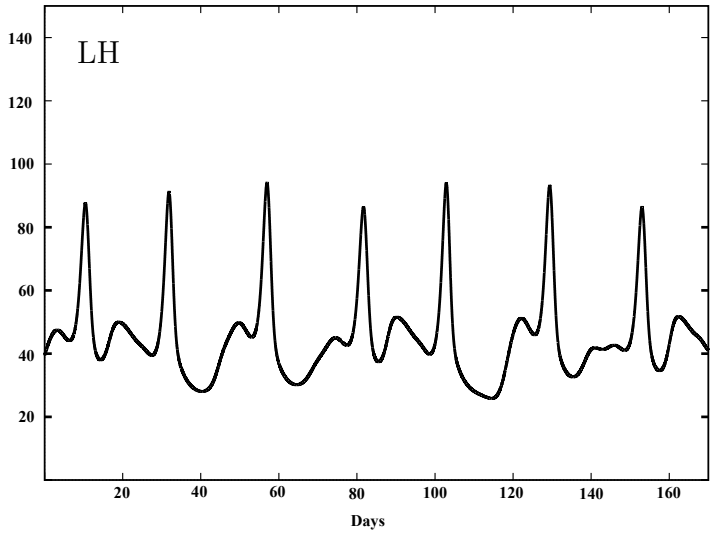

Figure 6.7: LH model simulations for eqs. 3.1 - 3.12 with zero time-delays. $\kappa = 1.15$ and the cycle is irregular with LH surges every 23 to 27 days.

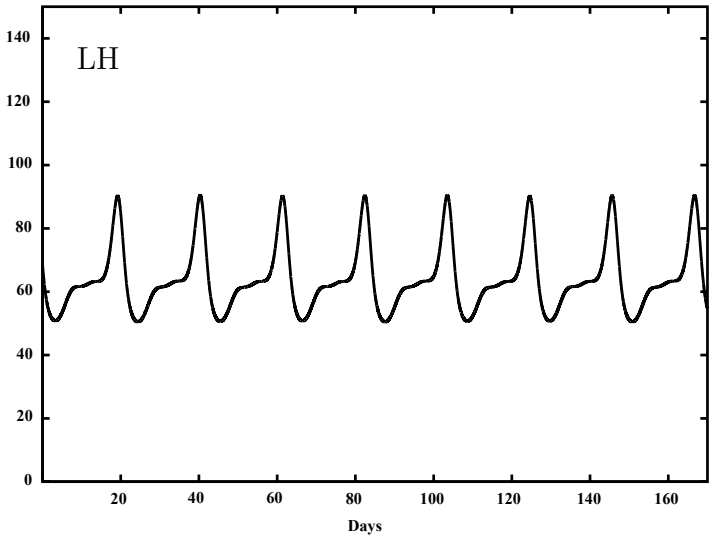

Figure 6.8: LH model simulations for $\kappa = 1.21$. The cycle has a period of 21 days and LH levels ranging between 50 IU/L and 92 IU/L.

6.4 Bifurcation Analysis for Parameters κ and t_3

To this point we have not identified a stable solution that exhibits a similar hormonal profile to that of classical PCOS, namely anovulatory and hyperandrogenic. In our sensitivity analysis parameters it is interesting to note, though they did not appear in our rankings, t_3 an t_4 have coefficients > 1. These represent the T produced by small antral ($SmAn$) and recruited (RcF) follicles in our auxiliary equation for T. In 1998, Nestler *et al.* showed that isolated theca cells from PCOS women demonstrated an approximately four fold increase in insulin stimulated T biosynthesis when compared with theca cells from normally cycling women [51]. Follicles harvested for their study ranged from between 4 mm an 12 mm in diameter, a range consistent with small antral and recruited follicle classifications. To investigate the possibility that multiple mechanisms of action may contribute to the etiology of classical PCOS, we again look at the bifurcation dynamics of κ, this time with varying rates of T production by small antral follicles ($SmAn$). The combined sensitivities of both t_3 and κ present a highly unpredictable 2-parameter analysis, given the numerical constraints of current software. Anticipating this challenge we begin our study using XPPAUT [21] as before, refining the mesh and step size to increase the accuracy of the analysis. First we look again at our κ bifurcation diagram with a slight increase in the value of t_3 from 0.67 to 0.75. The refined approach immediately reveals another significant bifurcation.

In contrast to the bifurcation diagram presented in Section 6.3, we notice an additional Hopf bifurcation appear within the line of unstable equilibria in Figure 6.9 at approximately $\kappa = 1.17$. This is the results of having two negative eigenvalues in addition to a complex pair that crosses the imaginary axis and results in the appearance of a line of unstable limit cycles. For reference we will further refer to the hysteresis loop

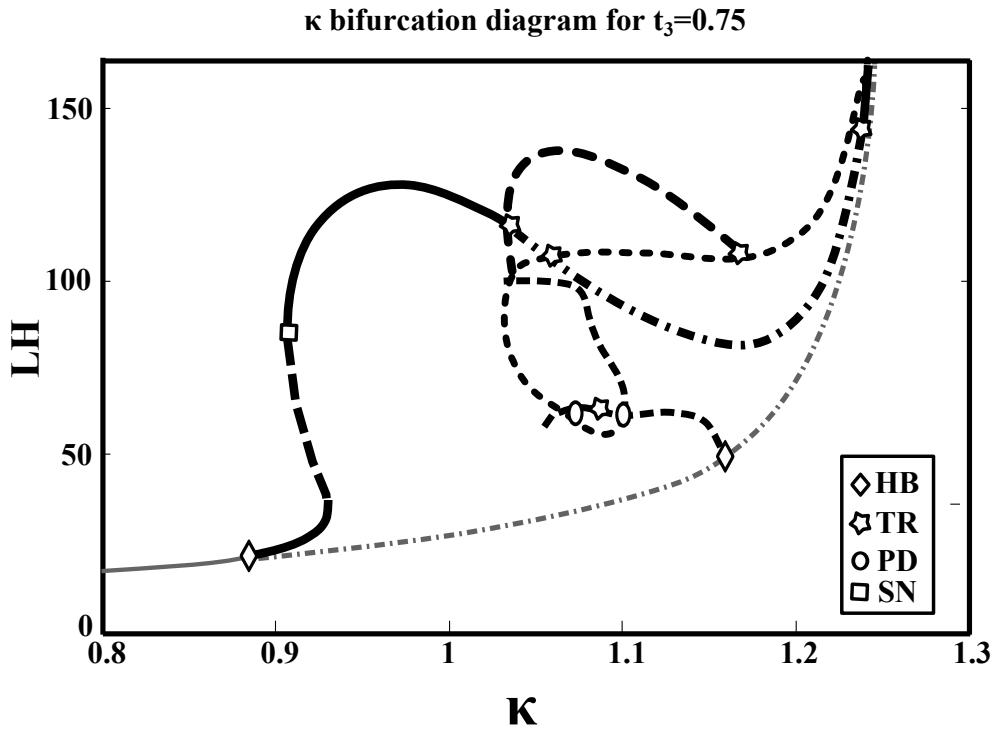

Figure 6.9: Bifurcation diagram with respect to κ, with $t_3 = 0.75$ for eqs. 3.1 - 3.12 with remaining parameters from $\tilde{\theta}$. HB, SN, TR and PD denote Hopf ($\diamond$), saddle-node ($\square$), torus ($\star$) and period doubling ($\circ$) bifurcations. Periodic solutions are represented in black with equilibria in gray. Stable solutions are presented with solid lines with dashed lines reflecting unstable solutions.

in Figure 6.5 as the "top branch" while any further solutions appearing from this new Hopf bifurcation will be referred to as on the "bottom branch". As before, this is a result of a pair of complex eigenvalues for the Jacobian within the neighborhood of $\kappa = 1.17$ crossing the imaginary axis. Initially, the newly found branch of unstable solutions begin to show an increased level of LH surge that travels left as κ decreases. We then identify a period doubling (PD) bifurcation. Briefly addresses in Chapter 5 Section 5.2, this is the first appearance of this phenomenon in regards to the parameter κ. These bifur-

cations occur when an eigenvalue of the return, or Poincaré map crosses the value -1 from above. Many times this behavior is referred to as leaving the unit circle. From this point, at approximately $\kappa = 1.1$, we notice two additional branches of unstable cycles emanate. The first branch, that tracks a quickly increasing LH level. The exact trajectory of this branch, as we approach the torus of our top branch, becomes suspect as it is not customary to observe such behavior. We will address this shortly.

On the lower amplitude branch of unstable period solutions, slightly further to the left, we encounter a Torus bifurcation. Analogous to the Hopf bifurcation for equilibria, a torus bifurcation occurs when the complex pair of eigenvalues for the return map of periodic cycles, cross the unit circle in the complex plane. If we continue to the left we quickly encounter an additional PD bifurcation, at $\kappa \approx 1.088$ that spawns two branches of unstable equilibria. One of which turns downward from the PD point and terminates in a narrow neighborhood of stable periodic solutions. The other branch turns upward, tracing values of κ that slowly begin to increase with the magnitude of the peak. This branch seems to reach a value of LH of approximately $110^{\text{U}}/_{\text{L}}$, until κ surpasses 1.3 where it takes a sharp turn parallel to the line of unstable equilibria at the lower right portion of the graph. During this plateau, we encounter two additional TR at $\kappa = 1.07$ and 1.18.

We reach the point in the diagram where it appears to display various crossings of unstable manifolds from our current perspective, when in fact each variation in dash patterns designate separate trajectories. An exact explanation for this is still being determined and requires much future work. One may speculate, that we are getting an indication to the shape of the torus from the top branch. For our current purposes though, the importance lies in the behavior of these trajectories as we increase the amount of T in the system on the lower branch of the diagrams.

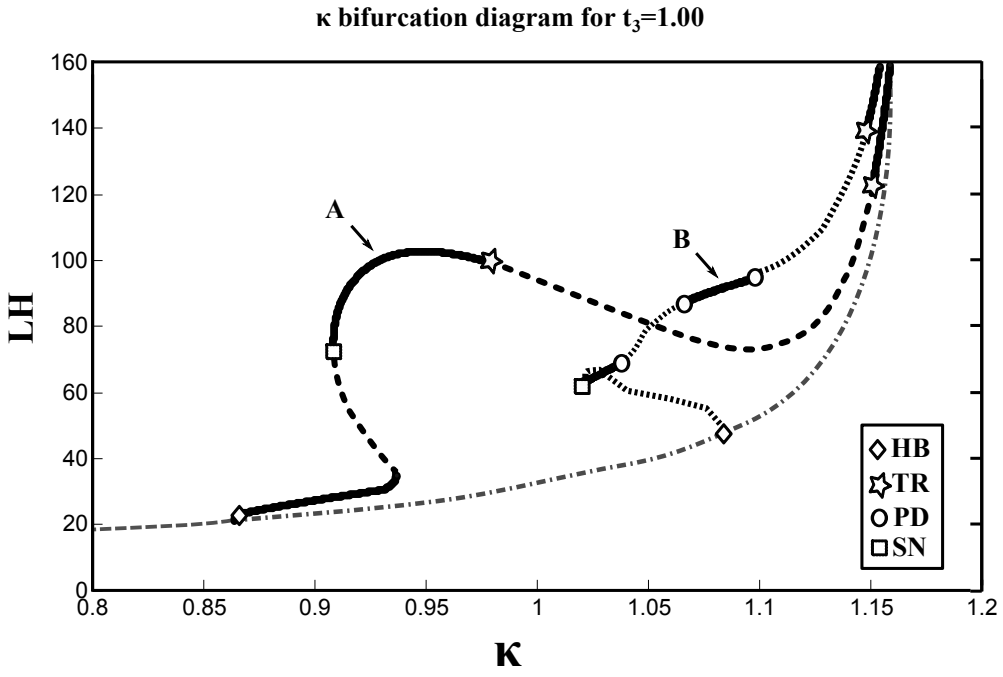

Figure 6.10: Bifurcation diagram with respect to κ, with $t_3 = 1.00$ for eqs. 3.1 - 3.12 with remaining parameters from $\tilde{\theta}$. HB, SN, TR and PD denote Hopf ($\diamond$), saddle-node ($\square$), torus ($\star$) and period doubling ($\circ$) bifurcations. Labeled points (A) and (B) designate location of solutions corresponding to LH profiles in Figure 6.11 (a) and (b) respectively

Figure 6.10 presents the diagram for κ that results from increasing the value of t_3 from 0.75 to 1.0. Stable solutions are shown in black, unstable in gray, with solid lines representing limit cycles and dashed lines reflecting equilibria. With this 25 % increase, we can begin to see a distinct change in the dynamics that stem from our second HB point. We no longer encounter a PD-TR-PD triplet of bifurcations at levels of LH around 50 $^{\text{U}}/_{\text{L}}$. This branch of unstable periodic solutions encounters a SN bifurcation, where it encounters a line of stable period cycles now both κ and LH begin to increase. We see a triplet now of all PD bifurcations that encase two short lines of stable periodic solutions. The top branch we saw in the original diagram persists, as does a stable periodic solution

that may be ovulatory. We examine a sample LH profile from a solution located at $\kappa = 0.94$ (A) in the diagram in Figure 6.11, panel (a). For comparison, we present the LH profile for a solution on the second branch of the diagram (see location (B)) in panel (b). As one can see, the increasing sensitivity to T begins to elevate our baseline LH and dampens the surge levels.

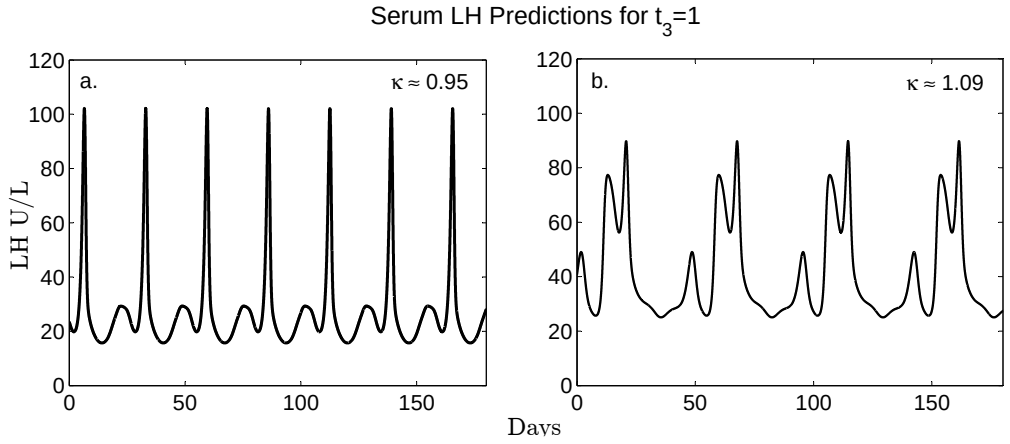

Figure 6.11: Serum LH predictions for Varying κ values with $t_3 = 1.00$. Panel (a) and (b) correspond to solutions at locations (A) and (B) respectively as identified in Figure 6.10, demonstrating the effects of increased sensitivity to T combined with elevated ovarian T production.

If we further increase our value for t_3 to 1.25 and analyze our κ dynamics we observe dramatic changes in the diagram. In Figure 6.10, given this new value for t_3, we notice the second Hopf bifurcation we first identified in Figure 6.9, was a degenerate and has split into two separate Hopf points. Instead of two branches of solutions that seem to intertwine, we notice a distinct line of stable equilibria between the remaining paths.

Refined examination of values of $t_3 \in (1, 1.25)$ have yet to definitively determine whether the top branch contracted, disappear, or joined with the smaller path. The appearance of a TR-TR-TR pattern of bifurcations seems to suggest we are looking at the remnants of a collapse in the top branch towards the line of unstable equilibria as it originally displayed that same pattern of bifurcations. Until further study resolves this debate, we focus on the resulting behavior of the remaining stable solutions.

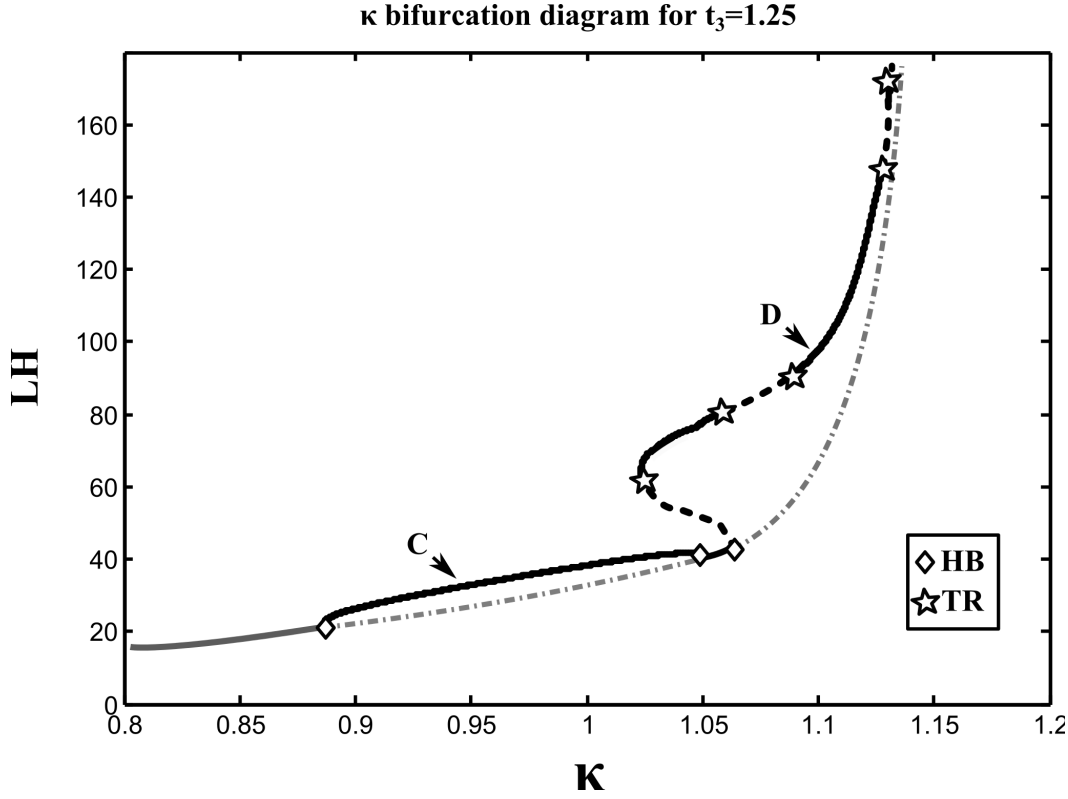

Figure 6.12: Bifurcation diagram with respect to κ, with $t_3 = 1.25$ for eqs. 3.1 - 3.12 with remaining parameters from $\tilde{\theta}$. HB and TR denote Hopf ($\diamond$) and torus ($\star$) bifurcations. Labeled points (C) and (D) designate location of solutions corresponding to LH profiles in Figure 6.11 (c) and (d) respectively

In Figure 6.13, we present LH profiles for solutions on both remaining paths of stable cycles. At $\kappa \approx 0.95$ (C) in Figure 6.12, we can see in Figure 6.13 panel (c) that sufficient surge levels for serum LH are not obtained. We observe low amplitude oscillations with a period of about 25 days. Our second point of interest in the bifurcation diagram is at $\kappa \approx 1.12$ (D) in Figure 6.12. Again the LH profile for this solution is presented for comparison in Figure 6.11 panel (d). Within the section of stable limit cycles, we can see the our baseline LH continues to increase with the values of t_3 while the range of LH values begins to contract.

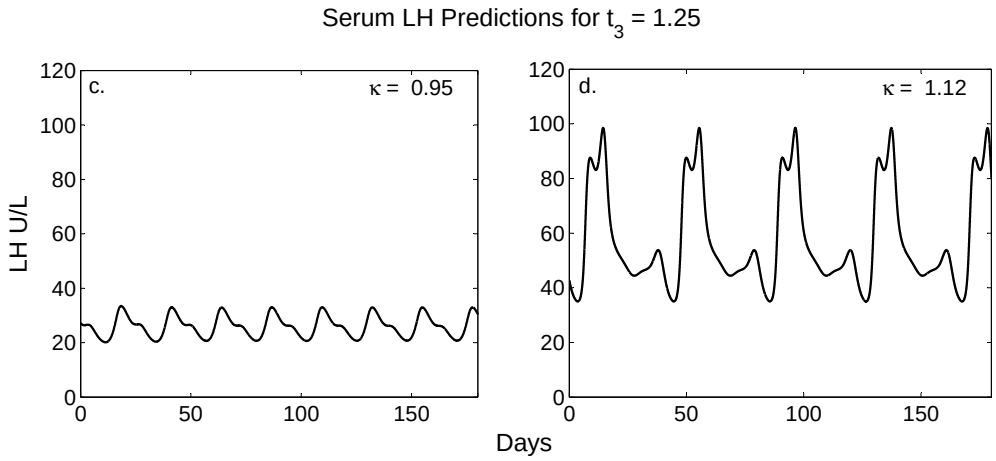

Figure 6.13: Serum LH predictions for Varying κ values with $t_3 = 1.25$. Panel (c) and (d) correspond to solutions at locations (C) and (D) respectively as identified in Figure 6.12, demonstrating the effects of increased sensitivity to T combined with elevated ovarian T production.

Increasing t_3 one additional time to 1.5, produces a κ bifurcation profile as represented

in Figure 6.14. We can see only small changes from the diagram for $t_3 = 1.25$. The range of κ for which solutions exist is slowly narrowing and our branch of stable limit cycles are expanding. The most significant change can not be seen on through the bifurcation diagram alone. If we take another look at a stable solution to the right of the TR at $\kappa \approx 1.11$, we can see that between $t_3 = 1.25$ and $t_3 = 1.5$ a significant change has taken place. In Figure 6.15, we present the serum hormone predictions for $t_3 = 1.5, \kappa = 1.12$ (see location (E) in Figure 6.14).

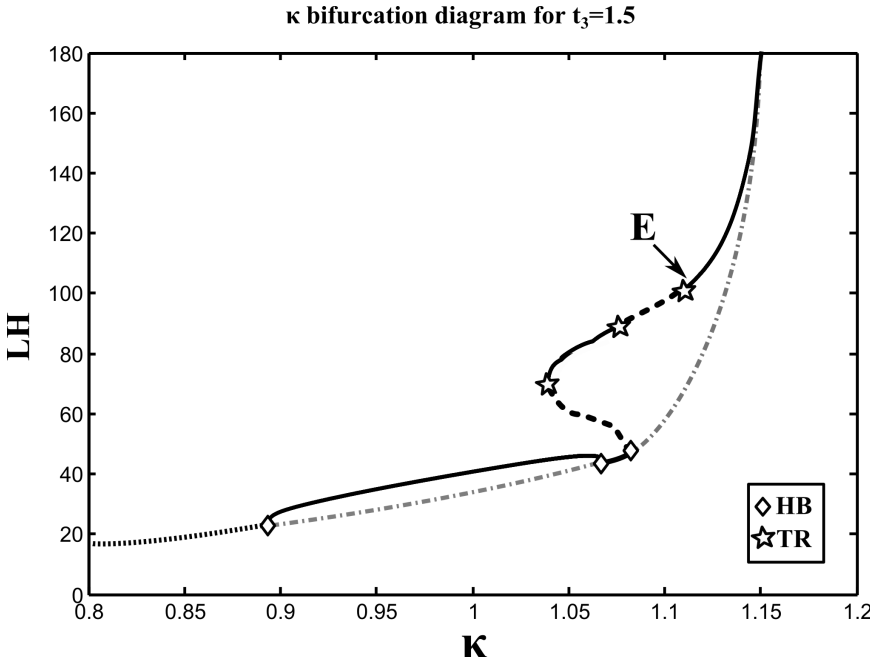

Figure 6.14: Bifurcation diagram with respect to κ, with $t_3 = 1.5$ for eqs. 3.1 - 3.12 with remaining parameters from $\tilde{\theta}$. HB and TR denote Hopf ($\diamond$) and torus ($\star$) bifurcations. Labeled point (E) designates location of solution corresponding to LH profiles in Figure 6.15.

For this solution, LH and T levels are consistently elevated. E2 and P4 levels are

suppressed reflecting a reduction in ovarian follicular activity. The elevation in circulating T is consistent with hyperandrogenic disorders. We can also take a brief look at the follicular dynamics for this solution in comparison to the normal cycle presented in Figure 6.1.

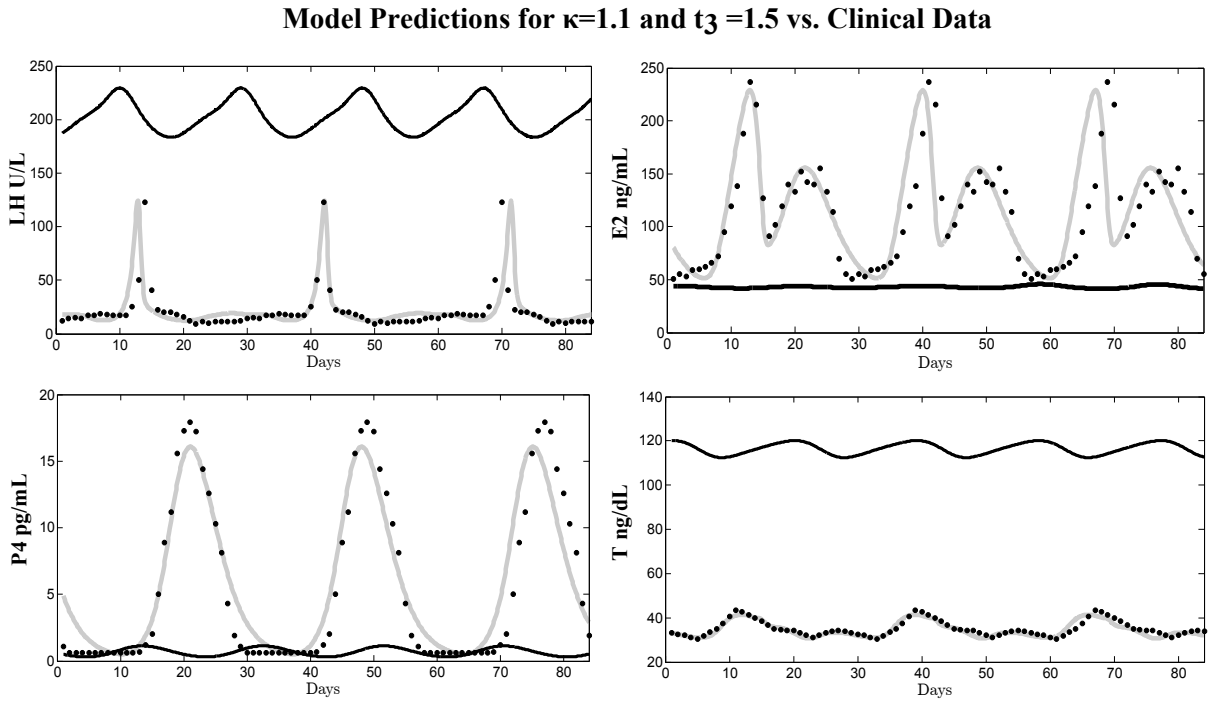

Figure 6.15: Serum LH predictions for$\kappa = 1.1$ with $t_3 = 1.5$. Predictions corresponds to solution at locations (E) as identified in Figure 6.14, demonstrating the effects of increased sensitivity to T combined with elevated ovarian T production.

In Figure 6.16 we present the predictions for ovarian mass of preantral ($PrA1$) and small antral ($SmAn$) follicles with a view of CL development ($Lut1$) for both the normal cycle (dashed lines) and the solution presented in Figure 6.15 (solid lines). One can see

that the mass of developing follicles for both classifications is significantly elevated, a case which may manifest in the appearance of polycystic ovaries on ultrasound. The CL, in this case is diminished, suggesting the absence of ovulation for the previous cycle. These predictions are the first we have seen through our investigations that reflect anovulatory and hyperandrogenic states simultaneously. These findings suggest multiple mechanisms may be implicated in disorders of this nature.

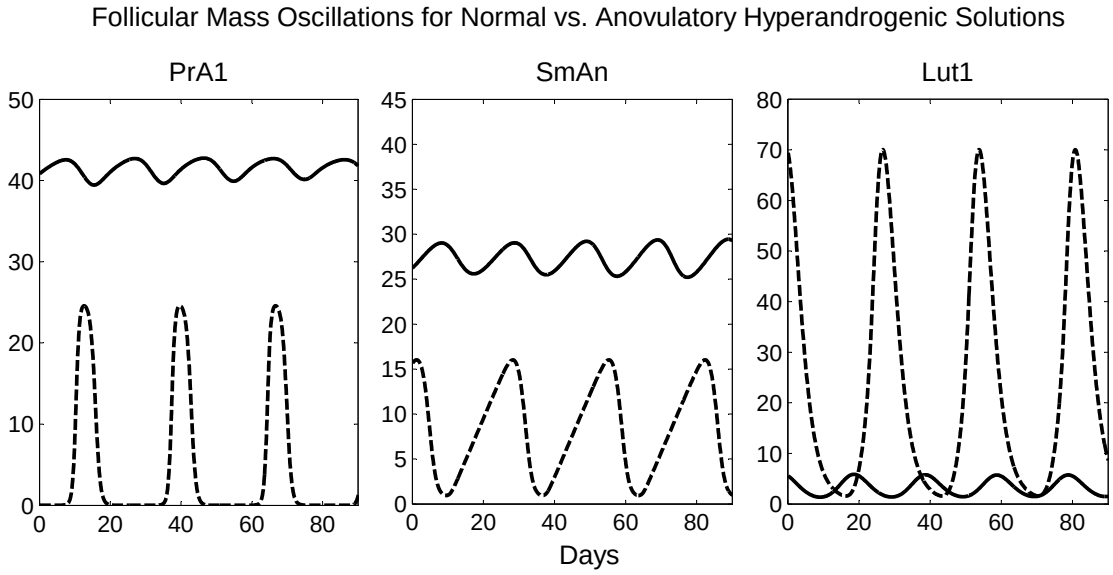

Figure 6.16: Ovarian mass predictions for $\kappa = 1.1$ values with $t_3 = 1.5$ (solid lines) compared with normal solution (dashed lines). Demonstrated is the significant increase in preantral and small antral follicular mass vs. normal, with decreased CL development.

Chapter 7

Summary and Future Directions

7.1 Commentary

After a short review of the physiological context of our study (Chapter 2), we have presented a nonlinear mechanistic model for the endocrine regulation of the human menstrual cycle which consists of 16 delay differential equations and 5 auxiliary equations, with 70 parameters, identified using data from literature (see Chapter 3). Using weighted least squares residuals and specialized data sampling, we have estimated 67 of our parameters that were not available in the literature (see Chapter 4). The complete model, with time delays for ovarian feedback, is shown to have a single stable periodic solution predicting serum levels of LH, FSH, E2, P4, InhA, InhB and T that is consistent with biological data [73, 84]. The asymptotically stable periodic solution resulting from the best fit parameter set (Appendix A.1 Tables 1 through 4) has a period of 29 days, consistent with current literature. Moreover, increases in qualitative accuracy are obtained through the use of mass action kinetic theory to describe preantral follicular through early antral follicular stage growth. We believe this is the first model of its type to be able to pre-

dict serum T levels in a mathematical context that allows analysis of bifurcations and multiple stable periodic solutions.

A benefit of this approach, is the identification of stable solutions that may resemble hormonal profiles consistent with some of the 16 PCOS phenotypes as defined in the Rotterdam consensus document [15]. While it is generally agreed that T plays an important role in PCOS, only 8 of the 16 PCOS phenotypes present with elevated androgens [15]. It is hypothesized that retarded preantral follicular development could play an important role in explaining the appearance of polycystic ovaries [44], a significant criterion in euandrogenic patients. Our approach of reflecting intra-ovarian follicular growth regulation systemically allows researchers to investigate effects of preantral growth abnormalities on menstrual cycle frequency. In our investigation, observations from increasing preantral follicle growth duration support the hypothesis presented by Maciel *et al.* [44] that a delay in early follicular maturation may be significant in the etiology of PCOS (see Chapter 5). Figures 5.4 through 5.7 reinforce this conclusion by demonstrating the reduction of m_2, that delays the transfer from preantral growth to androgen dependent growth, results in irregular cyclicity and a visible "stockpiling" of follicular mass in the preantral stages of development [44].

Furthermore, the identification of a period doubling cascade of bifurcations leading to chaotic behavior, may actually increase accuracy in representing clinical findings of women with PCOS and/or oligomenorrhea over previous models (see Chapter 5). A recent paper by Derry and Derry [17] presents a time series analysis of longitudinal menstrual cycle length data for 40 women over 20-40 years. They concluded that the human "menstrual cycle is the result of chaos in a nonlinear dynamical system" [17]. They further referenced specifically the model of Harris-Clark *et al.* [33] with the assertion that "any model producing only perfectly periodic menstrual cycles is, at best, incomplete" [17].

It is our belief that our current approach, meets their criteria for a model of the human menstrual cycle that displays biologically relevant random behavior independent of external interference. It also shows that follicular dynamics cannot be abandoned in the quest for accuracy, rather it is the interplay between intra-ovarian mass and endocrine regulation that explains this behavior. A formal bifurcation analysis of the period doubling bifurcation with respect to m_2, in Chapter 6 Section 6.2, suggests careful manipulation of preantral follicle growth may contribute to restoring ovulation in women with decreased LH profiles. Using XPPAUT, we confirm the existence of a period doubling cascade consistent with the existence of a chaotic attractor for the system without time delays. Further investigations of bifurcation dynamics for the parameter κ are presented. Our first investigation reveals a hysteresis loop of limit cycles that coalesces with an invariant torus. Solutions on the torus resemble ovulatory cycles that become increasingly irregular, suggesting the existence of an additional chaotic attractor that may more accurately represent an average, normally cycling woman. As a hyperandrogenic and anovulatory solution was yet to be identified, we present a series of bifurcation diagrams with respect to κ. Each diagram presented is evaluated for increasing levels of t_3 to represent an increased production of T by small antral follicles as reported by Nestler *et al.* [51]. Through these diagrams, we present the changes in dynamics that result from perturbations in two parameters and the effects on serum hormone level predictions at sample limit cycles. This investigation cumulates in the presentation of a hormone profile that is both hyperandrogenic and anovulatory. This may suggests that for women with classic PCOS, as reviewed in Chapter 2, that abnormalities in multiple physiological mechanisms may be intrinsic to the etiology of PCOS.

7.2 Future Work

We anticipate the emerging collaborations with clinical endocrinologists and experimentalists will soon provide essential data necessary to refine additional parameter sets that can simulate additional PCOS phenotypes. We are currently working on a merger of the presented model with previous work in glucoregulatory modeling, with the goal to increase our understanding of the relationship between disorders of reproduction and glucose metabolism. Funding opportunities are being sought to identify a model from glucose regulation and reproductive function in old world primates, from which our collaborators hope to find new areas of research for applications in infertility, obesity and Type II diabetes.

On an immediate note, during our investigations for this work, an additional chaotic attractor was identified at $\kappa = 1.09$ with $t_3 = 1$. This is within the "unknown" area of our κ bifurcation study.

The solution presented in Figure 7.1 is capable of producing ten ovulatory cycles per year. This may be an irregular solution on the invariant torus or a unique chaotic attractor, additional investigations are necessary to determine the exact nature of the state space in that region. With an average cycle length of 33 days for the 50 % threshold level, this profile may more accurately reflect what real women experience and could clinically be considered "normal". Mathematically, it is desirable to analyze the state space of this region as the opportunities to study the potential destabilization of a torus bifurcation to chaos through what seems to be a period doubling cascade.

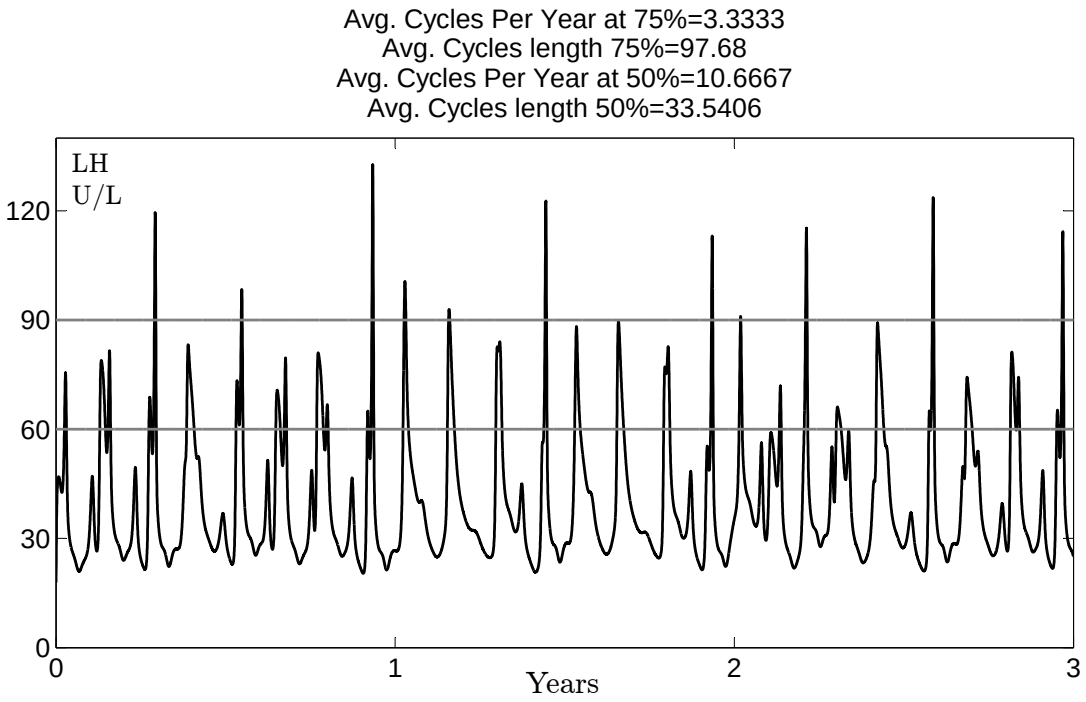

Figure 7.1: LH serum profile over 3 years is presented for an apparently chaotic attractor that may ovulate normally given the ovulatory follicle's sensitivity to LH

7.3 Conclusion

The basic assumption that the hypothalamic-pituitary-ovarian axis is in itself a closed autonomous dynamical system presenting stable yet chaotic behavior has led us to the development and presentation of our current model of endocrine regulation in female reproduction. Our model reflects pituitary synthesis and release of LH and FSH. Using an innovative combination of mass action and linear effects, we are able to mimic ovarian follicular growth patterns from which we approximate ovarian hormones. Numerical approximation of a stable periodic solution can be conducted in a matter of a few minutes as compactness was a major consideration in model development. These attributes make

it a prime candidate for *in-silico* investigations of cycle regularity. We have shown that modeling biological mechanisms, while considering clinical challenges and computational costs can lead to mathematically rich dynamics that present new model-derived insights that may guide future development of innovative individualized therapeutic interventions for women with PCOS. Furthermore, the implications of the presented bifurcation analysis suggest directions for pharmaceutical interventions that may lead to new treatments for PCOS. This type of analysis would not have been possible for systems of much higher dimensions than our own. As we move on towards further understanding of systems physiology, overcoming the temptation to unnecessarily complicate models serves an important purpose. It is our complete intention to continue on this path, building efficient models in systems physiology that maintain a balance between capturing the most significant mechanisms at play while maintaining the ability to analyze the phase space in the search of new frontiers.

REFERENCES

[1] F. Alvarez-Blasco, J. I. Botella-Carretero, and et al. JL San Millan. Prevalence and characteristics of the polycystic overy syndrome in overweight and obese women. *Archives of Internal Medicine*, 166:2081–2086, 2006.

[2] R. Azziz. Androgen excess is the key element in polycystic ovary syndrome. *Fertility and Sterility*, 80(2):252–254, Aug. 2003.

[3] R. Azziz. Androgen Excess in Women: Experience with Over 1000 Consecutive Patients. *Journal of Clinical Endocrinology & Metabolism*, 89(2):453–462, Feb. 2004.

[4] R. Azziz, E. Carmina, D. Dewailly, E. Diamanti-Kandarakis, H. F. Escobar-Morreale, W. Futterweit, O. E. Janssen, R. S. Legro, R. J. Norman, A. E. Taylor, and S. F. Witchel. The Androgen Excess and PCOS Society criteria for the polycystic ovary syndrome: the complete task force report. *Fertility and Sterility*, 91(2):456–488, 2009.

[5] R. Azziz, K. S. Woods, R. Reyna, T. J. Key, E. S. Knochenhauer, and B. O. Yildiz. The prevalence and features of the polycystic ovary syndrome in an unselected population. *The Journal of Clinical Endocrinology & Metabolism*, 89(6):2745–9, June 2004.

[6] A. R. Baerwald, G. P. Adams, and R. a. Pierson. A new model for ovarian follicular development during the human menstrual cycle. *Fertility and Sterility*, 80(1):116–122, July 2003.

[7] A. R. Baerwald, G. P. Adams, and R. a. Pierson. Ovarian antral folliculogenesis during the human menstrual cycle: a review. *Human reproduction update*, 18(1):73–91, 2011.

[8] R. T. Baird, R. Horton, C. Longcope, and J. F. Tait. Steroid dynamics under steady-state conditions. *Recent Progress in Hormone Research*, 25:611–664, 1969.

[9] H. T. Banks, M. Davidian, and S. J. R. An Inverse Problem Statistical Methodology Summery. Technical report, North Carolina State University, Raleigh, NC, 2007.

[10] R. M. Blair, H. Fang, W. S. Branham, B. S. Hass, S. L. Dial, C. L. Moland, W. Tong, L. Shi, R. Perkins, and D. M. Sheehan. The estrogen receptor relative binding affinities of 188 natural and xenochemicals: structural diversity of ligands. *Toxicological sciences : an official journal of the Society of Toxicology*, 54(1):138–53, Mar. 2000.

[11] S. K. Blank, C. R. McCartney, and J. C. Marshall. The origins and sequelae of abnormal neuroendocrine function in polycystic ovary syndrome. *Human Reproduction Update*, 12(4):351–361, July 2006.

[12] R. J. Bogumil, M. Ferin, J. Rootenberg, L. Speroff, and R. L. Vande Wiele. Mathematical studies of the human menstrual cycle. I. Formulation of a mathematical model. *The Journal of Clinical Endocrinology & Metabolism*, 35(1):126–43, July 1972.

[13] E. Carmina. The spectrum of androgen excess disorders. *Fertility and sterility*, 85(6):1582–5, June 2006.

[14] Y. D. Coble, P. O. Kohler, C. M. Cargille, and G. T. Ross. Production rates and metabolic clearance rates of human follicle-stimulating hormone in premenopausal and postmenopausal women. *The Journal of clinical investigation*, 48(2):359–63, Feb. 1969.

[15] T. R. E.-S. P. Consensus workshop group. 2004 Rotterdam 1: revised 2003 consensus on diagnostic criteria and long-term health risks related to polycystic ovary syndrome (PCOS). *Human Reproduction*, 19(1):41–47, 2004.

[16] V. De Leo and G. Morgante. Hormonal Effects of Flutamide in Young Women with Polycystic Ovary Syndrome. *Journal of Clinical Endocrinology and Metabolism*, 83(1):99–102, 1998.

[17] G. Derry and P. Derry. Characterization of chaotic dynamics in the human menstrual cycle. *Nonlinear Biomedical Physics*, 4(1):5, Jan. 2010.

[18] C. A. Eagleson, M. B. Gingrich, C. L. Pastor, T. K. Arora, C. M. Burt, W. S. Evans, and J. C. Marshall. Polycystic Ovarian Syndrome: Evidence that Flutamide Restores Sensitivity of the Gonadotropin-Releasing Hormone Pulse Generator to Inhibition by Estradiol and Progesterone. *Journal of Clinical Endocrinology & Metabolism*, 85(11):4047–4052, 2000.

[19] B. Efron and R. J. Tibshirani. *An Introduction to the Bootstrap*. Chapman & Hall, Boca Raton, FL, 1993.

[20] D. a. Ehrmann. Polycystic ovary syndrome. *The New England journal of medicine*, 352(12):1223–36, Mar. 2005.

[21] B. Ermentrout. *Simulating, Analyzing and Animating Dynamical Systems*. SIAM, Philadelphia, 2002.

[22] M. Eslami. *Theory of sensitivity in dynamical systems: An introduction*. Spring Verlag, Berlin, Germany, 1994.

[23] B. C. Fauser and A. M. Van Heusden. Manipulation of human ovarian function: physiological concepts and clinical consequences. *Endocrine Review*, 18(1)(1):71–106, Feb. 1997.

[24] B. C. J. M. Fauser, T. D. Pache, S. W. J. Lamberts, W. I. M. C. J. Hop, F. H. De Jong, and K. D. Dahl. Serum Bioactive and Immunoreactive Luteinizing Hormone and Follicle-Stimulating Hormone Levels in Women with Cycle Abnormalities, with or without Polycystic Ovarian Disease. *Journal of Clinical Endocrinology & Metabolism*, 73(4):811–817, Oct. 1991.

[25] A. F. Fihri, K. H. Hajji, and H. Lakhdissi. Histological exploration of follicular population of the Moroccan bovine (Oulmes-Zaers) breed. *African Journal of Biotechnology*, 3(May):294–298, 2004.

[26] P. Frank. *Introduction to sensitivity theory.* Acedemic Press, New York, NY, 1978.

[27] S. Franks. Polycystic Ovary Syndrome. *New England Journal of Medicine*, 333:853–861, 1995.

[28] S. Franks, D. White, C. Gilling-Smith, A. Carey, D. Waterworth, and R. Williamson. Hypersecretion of androgens by polycystic ovaries: the role of genetic factors in the regulation of cytochrome P450c17 alpha. *Baillière's clinical endocrinology and metabolism*, 10(2):193–203, Apr. 1996.

[29] W. Futterweit and L. Deligdisch. Histopathological Effects of Exogenously Administered Testosterone in 19 Female to Male Transsexuals. *Journal of Clinical Endocrinology & Metabolism*, 62(1):16–21, Jan. 1986.

[30] C. Gnoth, P. Frank-Herrmann, E. Schmoll, and G. Freundl. Cycle characteristics after discontinuation of oral contraceptives. *Gynecological Endocrinology*, 16(4):307–317, 200.

[31] A. Gougeon. Dynamics of follicular growth in the human: a model from preliminary results. *Human Reproduction (Oxford, England)*, 1(2):81–7, Feb. 1986.

[32] D. J. Haisenleder, L. L. Burger, K. W. Aylor, a. C. Dalkin, H. E. Walsh, M. a. Shupnik, and J. C. Marshall. Testosterone stimulates follicle-stimulating hormone beta transcription via activation of extracellular signal-regulated kinase: evidence in rat pituitary cells. *Biology of reproduction*, 72(3):523–9, Mar. 2005.

[33] L. Harris-Clark, P. M. Schlosser, and J. F. Selgrade. Multiple stable periodic solutions in a model for hormonal control of the menstrual cycle. *Bulletin of Mathematical Biology*, 65(1):157–73, Jan. 2003.

[34] S. G. Hillier and G. T. Ross. Effects of exogenous testosterone on ovarian weight, follicular morphology and intraovarian progesterone concentration in estrogen-primed hypophysectomized immature female rats. *Biology of Reproduction*, 20:261–268, 1979.

[35] J. Hotchkiss, D. J. Dierschke, W. R. Butler, G. R. Fritz, and E. Knobil. Relation between levels of circulating ovarian steroids and pituitary gonadotropin content during the menstrual cycle of the rhesus monkey. *Biology of reproduction*, 26(2):241–8, Mar. 1982.

[36] S. Jonard and D. Dewailly. The follicular excess in polycystic ovaries, due to intraovarian hyperandrogenism, may be the main culprit for the follicular arrest. *Human Reproduction Update*, 10(2):107–17, Jan. 2004.

[37] J. Keener and J. Sneyd. *Mathematical Physiology I: Cellular Physiology*. Springer-Verlag, New York, second edition, 2009.

[38] P. O. Kohler, G. T. Ross, and W. D. Odell. Metabolic clearance and production rates of human luteinizing hormone in pre- and postmenopausal women. *The Journal of clinical investigation*, 47(1):38–47, Jan. 1968.

[39] S.-W. Kuo, F.-C. Ke, G.-D. Chang, M.-T. Lee, and J.-J. Hwang. Potential role of follicle-stimulating hormone (FSH) and transforming growth factor (TGFβ1) in the regulation of ovarian angiogenesis. *Journal of Cellular Physiology*, 226(6):1608–19, June 2011.

[40] Y. a. Kuznetsov. *Elements of Applied Bifurcatino Theory*. Spinger, New York, NY, 1995.

[41] A. Lass. The role of ovarian volume in reproductive medicine. *Human Reproduction Update*, 5(3):256–266, May 1999.

[42] Y. S. S. Liu JH. Induction of midcycle surge by ovarian steriods in women: A critical evaluation. *Journal of Clinical Endocrinology*, 57(4):797–802, 1983.

[43] M. C. Lucy. Growth hormone regulation of follicular growth. *Reproduction, Fertility, and Development*, 24(1):19–28, Dec. 2011.

[44] G. A. R. Maciel, E. C. Baracat, J. A. Benda, S. M. Markham, K. Hensinger, R. J. Chang, and G. F. Erickson. Stockpiling of transitional and classic primary follicles in ovaries of women with polycystic ovary syndrome. *The Journal of Clinical Endocrinology & Metabolism*, 89(11):5321–7, Nov. 2004.

[45] A. Margolskee and J. F. Selgrade. Dynamics and bifurcation of a model for hormonal control of the menstrual cycle with inhibin delay. *Mathematical Biosciences*, 234(2):95–107, Dec. 2011.

[46] Matlab. *version 7.14 (R2012a)*. The MathWorks Inc., Natick, Massachusetts, 2012.

[47] R. McLachlan, N. Cohen, K. Dahl, W. Bremner, and M. Soules. Serum inhibin levels during the periovulatory interval in normal women: Relationships with sex steroid and gonadotrophin levels. *Clinical Endocrinology*, 1(32):39–48, 1990.

[48] F. Medina and J. Nestler. Insulin Stimulates Testosterone Biosynthesis by Human Theca Cells from Women with Polycystic Ovary Syndrome by Activating its own receptor and using inositoglycan mediators as the signal transduction system. *Journal of Clinical Endocrinology & Metabolism*, 83(6):2001–2005, 1998.

[49] P. Melrose and L. Gross. Steroid Effects on the Secretory Modalities of Gonadotropin-Releasing Hormone Release. *Endocrinology*, 121(1):190–199, July 1987.

[50] J. Naimark. Motions close to doubly asymptotic motions. *Solviet Math. Dokl.*, 8:221–231, 1967.

[51] J. E. Nestler. Insulin Stimulates Testosterone Biosynthesis by Human Thecal Cells from Women with Polycystic Ovary Syndrome by Activating Its Own Receptor and Using Inositolglycan Mediators as the Signal Transduction System. *Journal of Clinical Endocrinology & Metabolism*, 83(6):2001–2005, June 1998.

[52] S. S. Nussey and S. A. Whitehead. *Endocrinology : An Integrated Approach*. Taylor & Francis, London, 2001.

[53] W. Odell. *The Reproductive System in Women*. Grune & Stratton, New York, 1979.

[54] S. R. Ojeda. Female Reproductive Function. In W. J. Kovacks and S. R. Ojeda, editors, *Textbook of Endocrine Physiology*, chapter 8, pages 194–238. Oxford University Press, New York, 6th edition, 2012.

[55] M. Orisaka, K. Tajima, B. K. Tsang, and F. Kotsuji. Oocyte-granulosa-theca cell interactions during preantral follicular development. *Journal of Ovarian Research*, 2(1):9, Jan. 2009.

[56] T. D. Pache, S. Chadha, L. J. G. Gooren, W. C. J. Hop, K. W. Jaarsma, H. B. R. Dommerholt, and B. Fauser. Ovarian morphology in long-term androgen-treated female to male transsexuals. A human model for the study of polycystic ovarian syndrome? *Histopathology*, 19(5):445–452, 1991.

[57] D. Panidis, D. Macut, D. Farmakiotis, D. Rousso, A. Kourtis, I. Katsikis, N. Spanos, M. Petakov, J. Bjekic, and S. Damjanovic. Indices of insulin sensitivity, beta cell function and serum proinsulin levels in the polycystic ovary syndrome. *European Journal of Obstetrics, Gynecology, and Reproductive Biology*, 127(1):99–105, July 2006.

[58] R. Pasteur. *A multiple-inhibin model for the human menstrual cycle*. PhD thesis, North Carolina State University, 2008.

[59] R. Pasteur and J. Selgrade. A deterministic, mathematical model for hormonal control of the menstrual cycle. In W. Dubitzky, J. Southgate, and H. Fu\ss, editors, *Understanding the Dynamics of Biological Systems: Lessons Learned from Integrative Systems Biology*, pages 38–58. Singer, London, 2011.

[60] J. Pielecka, S. D. Quaynor, and S. M. Moenter. Androgens increase gonadotropin-releasing hormone neuron firing activity in females and interfere with progesterone negative feedback. *Endocrinology*, 147(3):1474–9, Mar. 2006.

[61] H. Poincaré. L'Équilibre d'une masse fluide animée d'un mouvement de rotation. *Acta Mathematica*, 7:259–380, 1885.

[62] P. Reddy, W. Zheng, and K. Liu. Mechanisms maintaining the dormancy and survival of mammalian primordial follicles. *Trends in Endocrinology and Metabolism*, 21(2):96–103, Feb. 2010.

[63] I. Reinecke and P. Deuflhard. A complex mathematical model of the human menstrual cycle. *Journal of Theoretical Biology*, 247(2):303–30, July 2007.

[64] S. Rice, K. Ojha, S. Whitehead, and H. Mason. Stage-specific expression of androgen receptor, follicle-stimulating hormone receptor, and anti-Müllerian hormone type II receptor in single, isolated, human preantral follicles: relevance to polycystic ovaries. *The Journal of clinical endocrinology and metabolism*, 92(3):1034–40, Mar. 2007.

[65] M. G. Ropelato, M. C. García Rudaz, M. E. Escobar, S. V. Bengolea, M. L. Calcagno, J. D. Veldhuis, and M. Barontini. Acute effects of testosterone infusion on the serum luteinizing hormone profile in eumenorrheic and polycystic ovary syndrome adolescents. *Journal of Clinical Endocrinology & Metabolism*, 94(9):3602–3610, 2009.

[66] R. J. Sacker. *On invariant surfaces and bifurcation of periodic solutions of ordinary differential equations*. New York University, IMM-NYU, New York, NY, 1964.

[67] E. Sander and J. Yorke. Connecting period-doubling cascades to chaos. *International Journal of Bifurcation and Chaos*, 22:1–29, 2012.

[68] M. Sar, D. B. Lubahn, F. S. French, and E. M. Wilson. Immunohistochemical Localization of the Androgen Receptor in Rat and Human Tissues. *Endocrinology*, 127(6):3180–3186, Dec. 1990.

[69] P. M. Schlosser and J. F. Selgrade. A model of gonadotropin regulation during the menstrual cycle in women: Qualitative features. *Environ. Health Perspect.*, 108(5):873–881, 2000.

[70] J. F. Selgrade, L. A. Harris, and R. D. Pasteur. A model for hormonal control of the menstrual cycle: Structural consistency but sensitivity with regard to data. *Journal of Theoretical Biology*, 260(4):572–580, Oct. 2009.

[71] J. F. Selgrade and P. M. Schlosser. A model for the production of ovarian hormones during the menstrual cycle. *Fields Institute Communications*, 21:429–446, 1999.

[72] A. Sen and S. R. Hammes. Granulosa Cell-Specific Androgen Receptors Are Critical Regulators of Ovarian Development and Function. *Molecular Endocrinology*, 24(7):1393–1403, July 2010.

[73] I. Sinha-Hikim, S. Arver, G. Beall, R. Shen, M. Guerrero, F. Sattler, C. Shikuma, J. C. Nelson, B. M. Landgren, N. a. Mazer, and S. Bhasin. The use of a sensitive equilibrium dialysis method for the measurement of free testosterone levels in healthy, cycling women and in human immunodeficiency virus-infected women. *The Journal of Clinical Endocrinology & Metabolism*, 83(4):1312–8, Apr. 1998.

[74] R. Sitruk-Ware. New progestagens for contraceptive use. *Human reproduction update*, 12(2):169–78, 2006.

[75] M. K. Skinner. Regulation of primordial follicle assembly and development. *Human Reproduction Update*, 11(5):461–471, 2005.

[76] T. Spinder, J. J. Spijkstra, J. G. Van Den Twel, C. W. Burger, H. Van Kessel, P. G. A. Hompes, and L. J. G. Gooren. The Effects of Long Term Testosterone Administration on Pulsatile Luteinizing Hormone Secretion and on Ovarian Histology in Eugonadal Female to Male Transsexual Subjects. *Journal of Clinical Endocrinology & Metabolism*, 69(1):151–157, July 1989.

[77] J. S. Stephen Franks and K. Hardy. Follicle dynamics and anovulation in polycystic ovary syndrome. *Human Reproductive Update*, 14(4):367–378, 2008.

[78] S. H. Strogatz. Exploring complex networks. *Nature*, 410(6825):268–76, Mar. 2001.

[79] H. Takeda, G. Chodak, S. Mutchnik, T. Nakamoto, and C. Chang. Immunohistochemical localization of androgen receptors with mono- and polyclonal antibodies to androgen receptor. *Journal of Endocrinology*, 126(1):17–NP, July 1990.

[80] A. Taylor, B. Mccourt, K. A. Martin, E. J. Anderson, J. M. Adams, D. Schoenfeld, and J. E. Hall. Determinants of abnormal gonadotropin secretion in clinically defined women with polycystic ovary syndrome. *Journal of Clinical Endocrinology & Metabolism*, 82(7):2248–2256, 1997.

[81] K. A. Vendola, J. Zhou, O. O. Adesanya, S. J. Weil, and C. A. Bondy. Androgens Stimulate Early Stages of Follicular Growth in the Primate Ovary. *The Journal of Clinical Investigation*, 101(12)(12):2622–2629, 1998.

[82] C. F. Wang, B. L. Lasley, A. Lein, and S. S. C. Yen. The Functional Changes of the Pituitary Gonadotrophs During the Menstrual Cycle. *Journal of Clinical Endocrinology & Metabolism*, 42(4):718–728, Apr. 1976.

[83] J. M. Weiss, S. S. Stojilkovic, K. Diedrich, O. Ortmann, and K. D. O. O. Juergen M. Weiss Stanko S. Stojilkovic. Effects of testosterone on hormonal content and calcium-dependent basal secretion in female rat pituitary cells. *Steriod Biology and Molecular Biology*, 103(2):149–157, Feb. 2007.

[84] C. K. Welt, D. J. McNicholl, A. E. Taylor, and J. E. Hall. Female reproductive aging is marked by decreased secretion of dimeric inhibin. *The Journal of Clinical Endocrinology & Metabolism*, 84(1):105–11, Jan. 1999.

[85] C. L. Westhoff, A. H. Torgal, E. R. Mayeda, M. C. Pike, and F. Z. Stanczyk. Pharmacokinetics of a combined oral contraceptive in obese and normal-weight women. *Contraception*, 81(6):474–80, June 2010.

[86] I. Wiegratz, K. Mittmann, H. Dietrich, T. Zimmermann, and H. Kuhl. Fertility after discontinuation of treatment with an oral contraceptive containing 30 microg of ethinyl estradiol and 2 mg of dienogest. *Fertility and sterility*, 85(6):1812–9, June 2006.

[87] M. Yasin, A. Dalkin, D. Haisenleder, and J. Marshall. Testosterone is required for gonadotropin-releasing hormone stimulation of luteinizing hormone-beta messenger ribonucleic acid expression in female rats. *Endocrinology*, 137(4), 1996.

[88] S. S. C. Yen, R. B. Jaffe, and R. L. Barbieri, editors. *The human menstrual cycle: Neuroendocrine regulation*, pages 191–217. W.B. Sauders Co., Philadelphia, 4th edition, 1999.

[89] A. J. Zeleznik. The physiology of follicle selection. *Reproductive Biology and Endocrinology*, 2:31, June 2004.

[90] R. Zhou, I. M. Bird, D. a. Dumesic, and D. H. Abbott. Adrenal hyperandrogenism is induced by fetal androgen excess in a rhesus monkey model of polycystic ovary

syndrome. *The Journal of clinical endocrinology and metabolism*, 90(12):6630–7, Dec. 2005.

APPENDICES

A.1 Best Fit Parameters ($\hat{\theta}$)

Table 1: LH Subsystem Parameters

Parameter	Value		Unit
$v_{0_{LH}}$	33.3	± 2	μ/day
$v_{1_{LH}}$	160.8	± 3.2	μ/day
Ki_{LH}	13.6	$\pm .2$	$L/nmol$
Km_{LH}	47.33	± 1.52	ng/L
k_{LH}	19.99	$\pm .48$	$1/day$
c_{LH_P}	0.982	$\pm 7.2E-05$	$L/nmol$
c_{LH_E}	0.9	$\pm 4E-04$	L/ng
d_P	1	$\pm 4.6E-05$	$days$
κ	0.917	$\pm 3.6E-04$	$dimensionless$
a	6.066	$\pm 1.2E-01$	$dimensionless$
δ	2		$dimensionless$
r_{LH}	14		$1/\text{day}$
v	2.5		$liters$

Estimated parameter values for LH subsystem parameters, corresponding to best fit solution, reported with estimates of standard deviation and units.

Table 2: FSH Subsystem Parameters

Parameter	Value		Unit
v_{FSH}	283.99	± 2.8	μ/day
Ki_{FSH_a}	6.380	± 0.089	μ/day
Ki_{FSH_b}	3000	± 227.9	L/nmol
k_{FSH}	3.646	± 0.0429	$1/\text{day}$
c_{FSH_p}	1.265	$\pm 1.245E-0.3$	L/nmol
c_{FSH_e}	0.055	$\pm 1.723E-03$	L/ng
ζ	1		$dimensionless$
d_{InhA}	1	$\pm 1.8E-05$	$days$
d_{InhB}	1	$\pm 2.9E-05$	$days$
r_{FSH}	8.210		$1/\text{day}$

Estimated parameter values for FSH subsystem parameters, corresponding to best fit solution, reported with estimates of standard deviation and units.

Table 3: Ovarian Subsystem Parameters

Parameter	Value		Unit
α	0.710	$\pm 1.3E-03$	*dimensionless*
β	0.693	$\pm 1.2E-03$	*dimensionless*
γ	$2E-04$	$\pm 4.2E-06$	*dimensionless*
η	1.162	$\pm 1.1E-03$	*dimensionless*
ν	8.000	$\pm 1.7E-01$	*dimensionless*
ϱ	0.450	$\pm 5.3E-03$	*dimensionless*
ι	0.950	$\pm 2.6E-04$	*dimensionless*
b	0.019	$\pm 7.4E-04$	$^{\mathrm{L}}/_{\mathrm{day}}$
c_1	0.087	$\pm 1.4E-03$	$^{\mathrm{L}}/_{\mu\mathrm{g}}$
c_2	0.125	$\pm 2.0E-03$	$^{1}/_{\mathrm{day}}$
c_3	0.053	$\pm 1.6E-03$	$^{1}/_{\mathrm{day}}$
c_4	0.037	$\pm 1.7E-03$	$^{1}/_{\mathrm{day}}$
c_5	0.481	$\pm 2.9E-03$	$^{1}/_{\mathrm{day}}$
d_1	0.705	$\pm 9.1E-04$	$^{1}/_{\mathrm{day}}$
d_2	0.649	$\pm 1.3E-03$	$^{1}/_{\mathrm{day}}$
k_1	0.709	$\pm 1.3E-03$	$^{1}/_{\mathrm{day}}$
k_2	0.871	$\pm 4.9E-04$	$^{1}/_{\mathrm{day}}$
k_3	1.038	$\pm 1.3E-04$	$^{1}/_{\mathrm{day}}$
k_4	1.052	$\pm 1.9E-04$	$^{1}/_{\mathrm{day}}$
m_1	0.927	$\pm 1.1E-03$	$^{1}/_{\mathrm{day}}$
m_2	$1.34E-03$	$\pm 9.9E-05$	$^{1}/_{\mathrm{day}}$
m_3	0.150	$\pm 5.7E-03$	$^{1}/_{\mathrm{day}}$
Km_{FSH}	7.530	$\pm 2.7E-01$	$^{1}/_{\mathrm{day}}$

Estimated parameter values for ovarian subsystem parameters, corresponding to best fit solution, reported with estimates of standard deviation and units.

Table 4: Auxiliary Equations Parameter Set

Parameter	Value		Unit
e_0	38.250	$\pm 2.9E+00$	$^{\mathrm{ng}}/_{\mathrm{L}}$
e_1	2.300	$\pm 8.4E-02$	$^{1}/_{\mathrm{kL}}$
e_2	2.724	$\pm 2.4E-02$	$^{1}/_{\mathrm{kL}}$
h_0	0.053	$\pm 6.4E-04$	$^{\mathrm{U}}/_{\mathrm{L}}$
h_1	0.025	$\pm 1.5E-03$	$^{\mathrm{nmol/L}}/_{\mu\mathrm{g}}$
h_2	0.063	$\pm 5.6E-04$	$^{\mathrm{U}}/_{\mathrm{L}}$
h_3	0.158	$\pm 5.1E-03$	$^{\mathrm{U}}/_{\mathrm{L}}$
p_1	0.255	$\pm 3.1E-03$	$^{\mathrm{nmol/L}}/_{\mu\mathrm{g}}$
p_2	0.128	$\pm 2.0E-03$	$^{\mathrm{nmol/L}}/_{\mu\mathrm{g}}$
j_0	27.21	$\pm 1.3E-03$	$^{\mathrm{pg}}/_{\mathrm{L}}$
j_1	1.885	± 2	$^{1}/_{\mathrm{L}}$
j_2	3.738	$\pm 6.7E-03$	$^{1}/_{\mathrm{L}}$
j_3	3.411	$\pm 1.3E-01$	$^{1}/_{\mathrm{L}}$
j_4	$2.06E-05$	$\pm 1.1E-01$	$^{1}/_{\mathrm{L}}$
j_5	3.000	$\pm 1.6E-06$	$^{1}/_{\mathrm{L}}$
j_6	0.001	$\pm 4.8E-02$	$^{1}/_{\mathrm{L}}$
t_0	21.920	$\pm 3.4E-05$	$^{\mathrm{ng}}/_{\mathrm{dL}}$
t_1	0.372	$\pm 7.3E-01$	$^{1}/_{\mathrm{dL}}$
t_2	0.296	$\pm 5.7E-03$	$^{1}/_{\mathrm{dL}}$
t_3	0.454	$\pm 1.9E-03$	$^{1}/_{\mathrm{dL}}$
t_4	0.041	$\pm 2.3E-03$	$^{1}/_{\mathrm{dL}}$
t_5	0.703	$\pm 4.7E-04$	$^{1}/_{\mathrm{dL}}$
t_6	$3.31E-08$	$\pm 1.5E-03$	$^{1}/_{\mathrm{dL}}$
t_7	0.046	$\pm 5.3E-04$	$^{1}/_{\mathrm{dL}}$
t_8	0.200	$\pm 1.7E-03$	$^{1}/_{\mathrm{dL}}$

Estimated parameter values for auxiliary equation parameters, corresponding to best fit solution, reported with estimates of standard deviation and units.

A.2 Clinical Data

Table 5: Daily Serum Hormone Levels From Literature

Welt *et al.*						Sinha-Hikim *et al.*
$LH^{\mu}/_{day}$	$FSH^{\mu}/_{\text{day}}$	$E2^{\text{ng}}/_{\text{L}}$	$P4^{\text{nmol/L}}/_{\mu\text{g}}$	$IHA^{\text{U}}/_{\text{L}}$	$IHB^{\text{pg}}/_{\text{L}}$	$T^{\text{ng}}/_{\text{dL}}$
12	11.4	51	1.1	1	79	33.2
14	11.6	55	0.6	1.1	109	32.5
15	11.7	53	0.6	1	116	32.0
14	12.4	59	0.6	1.1	123	31.1
17	12.6	60	0.6	1.1	140	30.3
17	11.3	62	0.6	1	135	31.6
19	12.1	66	0.6	1.1	140	33.4
18	11.3	72	0.6	1.2	144	35.0
17	10	95	0.6	1.7	147	37.5
17	8.7	119	0.6	2.3	130	40.7
17	8.6	138	0.6	3.2	113	43.4
25	8.2	188	0.6	4.5	98	42.6
50	10.4	237	0.7	7.4	83	41.4
123	19.6	215	1.2	9.3	147	39.9
41	12.1	127	2	7.7	167	38.4
22	9.2	91	5	8.1	106	36.6
20	8.7	102	8.9	10.1	57	34.9
20	8.6	119	11.2	8.9	44	34.6
18	7.4	140	15.6	9.5	43	34.4
16	7.2	133	17.3	11.5	38	34.3
12	6.1	152	17.9	9.1	32	33.4
9	5.4	142	17.2	8.7	30	32.3
11	5.2	140	14.4	7.5	29	31.1
10	5.4	155	12.6	6.6	36	32.0
11	5.3	133	10.3	5.7	30	33.2
11	6.1	114	8.1	4.1	37	33.9
11	6.7	70	4.3	2.2	35	34.4
11	8.3	55	1.9	1.7	55	34.0

Daily values for serum hormones over a single 28 day cycle as extracted using *Digitizeit* from Welt *et al.* [84] and Sinha-Hikim *et al.* [73].

A.3 Sensitivities

Table 6: Top 10 Most Sensitive Parameters

Parameter	Average	E2 Peak	LH Peak	T Peak
β	7.8	6.4	13	3.9
c_1	2.9	2.9	3.7	1.9
κ	2.7	4	2.2	2
V_{FSH}	2.3	2.6	2.7	1.7
k_{LH}	1.9	1.6	3.1	0.98
c_{LH_E}	1.7	1.3	2.7	0.88
c_3	1.6	0.8	3.1	0.85
ι	1.4	2.	1.4	0.059
α	1.2	1.9	0.037	1.
p_1	1.1	0.79	1.9	0.5

Highest ranking parameter in regards to average sensitivity for three biologically significant data points; E2 peak, LH peak, and T peak.

Table 7: Pituitary System Sensitivity Coefficients For Best Fit Solution

Parameter	**E2 peak**	**LH peak**	**T peak**
$v_{0_{LH}}$	1.04	1.04	0.51
$v_{1_{LH}}$	$1.3E-01$	0.26	$6.0E-02$
Ki_{LH}	0.20	0.78	0.16
Km_{LH}	0.26	0.37	0.15
k_{LH}	1.55	3.07	0.98
c_{LH_P}	0.38	0.74	0.25
c_{LH_E}	1.35	2.73	0.88
d_P	$8.0E-02$	0.16	$5.4E-02$
$kappa$	3.99	2.17	2.00
a	$3.9E-02$	$5.0E-02$	$2.3E-02$
$delta$	0.31	1.15	0.19
V_{FSH}	2.56	2.73	1.70
Ki_{FSH_a}	0.27	1.03	0.18
Ki_{FSH_b}	$8.2E-02$	$6.4E-02$	$5.6E-02$
k_{FSH}	0.78	1.32	0.54
c_{FSH_P}	0.30	0.51	0.23
c_{FSH_E}	0.81	1.40	0.55
$zeta$	4.83	8.26	3.91
d_{IHA}	$2.1E-02$	$4.3E-02$	$2.5E-02$
d_{IHB}	$7.9E-04$	$2.8E-02$	$4.5E-04$

Table 8: Ovarian System Sensitivity Coefficients For Best Fit Solution

Parameter	**E2 peak**	**LH peak**	**T peak**
$alpha$	1.9	$3.7E-02$	1.7
$beta$	6.4	13.1	3.9
$gamma$	$1.0E-03$	$1.1E-02$	$3.8E-04$
eta	0.14	0.25	0.96
nu	$1.7E-02$	$7.4E-02$	$9.7E-03$
$varrho$	0.15	0.18	$7.4E-02$
$iota$	2.8	1.4	$5.9E-02$
b	0.14	0.17	$6.7E-02$
c_1	2.9	3.7	2.0
c_2	1.0	0.21	0.93
c_3	0.79	3.1	0.85
c_4	0.79	0.96	0.20
c_5	0.35	0.80	0.26
d_1	0.20	0.35	0.11
d_2	0.20	0.39	0.11
k_1	0.24	0.50	0.15
k_2	0.25	0.61	0.15
k_3	0.23	0.53	0.15
k_4	$5.2E-02$	0.25	$4.4E-02$
m_1	0.41	0.36	0.19
m_2	$1.6E-02$	0.09	$1.4E-02$
m_3	$7.2E-02$	0.17	$4.6E-02$
Km_{FSH}	0.31	0.86	0.23

Table 9: Auxiliary Sensitivity Coefficients for $\hat{\theta}$

Parameter	**E2 peak**	**LH peak**	**T peak**
e_0	0.21	0.20	$4.5E-02$
e_1	1.3	1.2	0.28
e_2	$2.0E-02$	$2.2E-02$	$4.4E-03$
h_0	$2.0E-02$	$6.8E-02$	$1.2E-02$
h_1	$7.5E-03$	0.11	$2.5E-03$
h_2	$4.8E-02$	0.19	0.04
h_3	$8.0E-02$	0.37	$6.9E-02$
p_1	0.79	1.90	0.50
p_2	0.23	0.67	0.16
j_1	$2.0E-02$	$6.1E-02$	$1.2E-02$
j_2	$3.0E-03$	$1.2E-02$	$1.7E-03$
j_3	$4.3E-02$	$6.0E-02$	$2.6E-02$
j_4	$3.2E-02$	$5.3E-02$	$2.4E-02$
j_5	$2.1E-03$	$1.6E-02$	$1.1E-03$
j_6	$3.5E-02$	$7.0E-02$	$2.5E-02$
j_7	$7.8E-05$	$7.0E-04$	$5.3E-05$
t_1	0.65	0.31	0.17
t_2	$3.8E-02$	$6.4E-02$	$2.7E-02$
t_3	0.21	0.34	0.12
t_4	0.29	$4.6E-02$	$7.9E-02$
t_5	$1.5E-02$	0.10	$7.6E-02$
t_6	$9.0E-02$	0.44	0.20
t_7	$4.4E-04$	$1.1E-02$	$1.1E-04$
t_8	$3.9E-02$	$8.1E-02$	$4.3E-02$
t_9	$8.0E-02$	0.23	$7.1E-02$

A.4 Testosterone Unit Conversion

The original data set identified for serum total T levels across the menstrual cycle was obtained from Sinha-Hikim *et al.* [73], reporting total serum testosterone levels between 0.8 and 1.8 $^{\text{nmol}}/_{\text{L}}$. For conversion to $^{\text{ng}}/_{\text{dL}}$ we first identify the molecular formula of T:

$$C_{19}H_{28}O_2.$$

The molecular weight is then calculated by:

$$\begin{aligned}\text{Molecular Mass of } C_{19}H_{28}O_2 &= (\#\text{Atoms of C} \times \text{Atomic Weight of C}) \\ &\quad + (\#\text{Atoms of H} \times \text{Atomic Weight of H}) \\ &\quad + (\#\text{Atoms of O} \times \text{Atomic Weight of O}) \\ &= (19 \times 12.0110) + (28 \times 1.0079) + (2 \times 15.9994) \\ &= 288.4290\ ^{\text{g}}/_{\text{mol}} \qquad (1)\end{aligned}$$

We scale the Sinha-Hikim data by a factor of 28.84290 to allow the use of $^{\text{ng}}/_{\text{dL}}$ for our units, avoiding values less than 1, and allowing comparison of blood hormone levels with data from Welt.

A.5 Non-Delay System Parameters $\tilde{\theta}$

Table 10: LH Zero Delay Subsystem Parameters

Parameter	Value	Unit
$v_{0_{LH}}$	39.75	$^{\mu}/_{\text{day}}$
κ	0.9176	*dimensionless*
$v_{1_{LH}}$	153.7	$^{\mu}/_{\text{day}}$
a	7.396	*dimensionless*
Ki_{LH}	13.64	$^{\text{L}}/_{\text{nmol}}$
Km_{LH}	52.07	$^{\text{ng}}/_{\text{L}}$
k_{LH}	18	$^{1}/_{\text{day}}$
c_{LH_P}	0.9824	$^{\text{L}}/_{\text{nmol}}$
c_{LH_E}	0.8082	$^{\text{L}}/_{\text{ng}}$
δ	2	*dimensionless*
r_{LH}	14	$^{1}/_{\text{day}}$
v_{FSH}	287.3	$^{\mu}/_{\text{day}}$
$Ki_{FSH_{INH_A}}$	6.3	$^{\mu}/_{\text{day}}$
$Ki_{FSH_{INH_B}}$	3000	$^{\text{L}}/_{\text{nmol}}$
k_{FSH}	3.863	$^{1}/_{\text{day}}$
c_{FSH_P}	1.261	$^{\text{L}}/_{\text{nmol}}$
c_{FSH_E}	$2.50E-04$	$^{\text{L}}/_{\text{ng}}$
ζ	2	*dimensionless*
a_{FSH}	8.21	$^{1}/_{\text{day}}$
v	2.5	L

Table 11: FSH Subsystem Zero Delay Parameters

Parameter	Value	Unit
v_{FSH}	287.3	μ/day
Ki_{FSH_a}	6.300	μ/day
Ki_{FSH_b}	3000	L/nmol
k_{FSH}	3.870	$1/\text{day}$
c_{FSH_p}	1.260	L/nmol
c_{FSH_e}	$2.50E-04$	L/ng
ζ	2.000	$dimensionless$
d_{InhA}	0.000	$days$
d_{InhB}	0.000	$days$
r_{FSH}	8.210	$1/\text{day}$

Table 12: Ovarian Subsystem Zero Delay Parameters

Parameter	Value	Unit
$alpha$	0.69	$dimensionless$
$beta$	0.693	$dimensionless$
$gamma$	0.002	$dimensionless$
eta	1.162	$dimensionless$
nu	8	$dimensionless$
$varrho$	0.45	$dimensionless$
$iota$	0.952	$dimensionless$
b	0.017	$^{\mathrm{L}}/_{\mathrm{day}}$
c_1	0.087	$^{\mathrm{L}}/_{\mu\mathrm{g}}$
c_2	0.115	$^{1}/_{\mathrm{day}}$
c_3	0.534	$^{1}/_{\mathrm{day}}$
c_4	0.368	$^{1}/_{\mathrm{day}}$
c_5	0.482	$^{1}/_{\mathrm{day}}$
d_1	0.706	$^{1}/_{\mathrm{day}}$
d_2	0.6515	$^{1}/_{\mathrm{day}}$
k_1	0.695	$^{1}/_{\mathrm{day}}$
k_2	0.872	$^{1}/_{\mathrm{day}}$
k_3	1.039	$^{1}/_{\mathrm{day}}$
k_4	1.052	$^{1}/_{\mathrm{day}}$
m_1	0.927	$^{1}/_{\mathrm{day}}$
m_2	$8.680E-04$	$^{1}/_{\mathrm{day}}$
m_3	0.09	$^{1}/_{\mathrm{day}}$
Km_{FSH}	6.53	$^{1}/_{\mathrm{day}}$

Table 13: Auxiliary Equations Zero Delay Parameter Set

Parameter	Value	Unit
e_0	37.400	$^{ng}/_{L}$
e_1	2.300	$^{1}/_{kL}$
e_2	2.720	$^{1}/_{kL}$
h_0	0.053	$^{U}/_{L}$
h_1	0.026	$^{nmol/L}/_{\mu g}$
h_2	0.064	$^{U}/_{L}$
h_3	0.160	$^{U}/_{L}$
p_1	0.255	$^{nmol/L}/_{\mu g}$
p_2	0.133	$^{nmol/L}/_{\mu g}$
j_0	0.001	$^{pg}/_{L}$
j_1	1.720	$^{1}/_{L}$
j_2	50.03	$^{1}/_{L}$
j_3	4.323	$^{1}/_{L}$
j_4	$1.19E-03$	$^{1}/_{L}$
j_5	2.250	$^{1}/_{L}$
j_6	0.001	$^{1}/_{L}$
t_0	13.14	$^{ng}/_{dL}$
t_1	0.041	$^{1}/_{dL}$
t_2	0.667	$^{1}/_{dL}$
t_3	0.744	$^{1}/_{dL}$
t_4	0.000	$^{1}/_{dL}$
t_5	0.097	$^{1}/_{dL}$
t_6	0.00	$^{1}/_{dL}$
t_7	0.210	$^{1}/_{dL}$
t_8	0.093	$^{1}/_{dL}$